

Regulation of developmental hierarchy in *Drosophila* neural stem cell tumors by COMPASS and Polycomb complexes

Cassandra Gaultier, Sophie Foppolo, Cédric Maurange*

COMPASS and Polycomb complexes are antagonistic chromatin complexes that are frequently inactivated in cancers, but how these events affect the cellular hierarchy, composition, and growth of tumors is unclear. These characteristics can be systematically investigated in *Drosophila* neuroblast tumors in which cooption of temporal patterning induces a developmental hierarchy that confers cancer stem cell (CSC) properties to a subset of neuroblasts retaining an early larval temporal identity. Here, using single-cell transcriptomics, we reveal that the *trithorax*/MLL1/2-COMPASS-like complex guides the developmental trajectory at the top of the tumor hierarchy. Consequently, *trithorax* knockdown drives larval-to-embryonic temporal reversion and the marked expansion of CSCs that remain locked in a spectrum of early temporal states. Unexpectedly, this phenotype is amplified by concomitant inactivation of Polycomb repressive complex 2 genes, unleashing tumor growth. This study illustrates how inactivation of specific COMPASS and Polycomb complexes cooperates to impair tumor hierarchies, inducing CSC plasticity, heterogeneity, and expansion.

Copyright © 2022
The Authors, some
rights reserved;
exclusive licensee
American Association
for the Advancement
of Science. No claim to
original U.S. Government
Works. Distributed
under a Creative
Commons Attribution
NonCommercial
License 4.0 (CC BY-NC).

INTRODUCTION

Most tumors are composed of a heterogeneity of cell states and cell types (1, 2). Intratumor heterogeneity can be caused by accumulating mutations, region-specific microenvironments, or infiltration by immune cells. In addition, recent studies suggest that the aberrant recapitulation of developmental programs, by creating hierarchies of cellular states, is also a robust driver of cellular heterogeneity in some cancers (3–6). The latter phenomenon likely contributes to the establishment of so-called cancer stem cells (CSCs). CSCs represent a subpopulation of tumor cells that lie at the apex of the cellular hierarchy. They drive tumor growth through a default unlimited proliferative potential while also being at the origin of the more differentiated cell types present in tumors (7). The mechanisms that restrain or favor progression throughout developmental hierarchies to balance CSC proliferation or differentiation remain poorly understood.

COMPASS and Polycomb group (PcG) complexes are evolutionarily conserved heteromultimeric chromatin complexes with antagonistic activities on gene transcription (8, 9). The COMPASS group comprises three main complexes: Set1A/B-COMPASS, MLL1/2-COMPASS-like, and MLL3/4-COMPASS-like (8, 10, 11). They mainly differ by distinct histone methyltransferases (Set1A/B, MLL1/2, and MLL3/4) that can deposit mono-, di-, or trimethylation marks on lysine 4 of histone H3 (referred to as H3K4) to sustain transcription. Each COMPASS complex can target different regions on the genome and distinct gene sets. For example, the *SET1/B-COMPASS* can promote all types of H3K4 methylation genome-wide, while MLL1/2-COMPASS-like-mediated di- and trimethylation appear to be restricted to the promoters of developmental genes. In contrast, the MLL3/4-COMPASS-like complex deposits H3K4 monomethylation marks at active enhancers. The three complexes have nonoverlapping

roles and are critical for development (10). Whereas H3K4 methylation by COMPASS complexes provides a permissive chromatin context for transcription, H3K27 methylation by the PcG represses transcription. The main H3K27 histone methyltransferase is Enhancer of zeste homolog 2 (EZH2) that belongs to the Polycomb repressive complex 2 (PRC2). The PRC1 complex lacks any H3K27 methyltransferase activity (11).

Molecular work suggests that PcG and COMPASS complexes share overlapping targets, a subset of them being important for development. In particular, PcG and the MLL1/2-COMPASS-like complexes are mutually antagonistic in *Drosophila* and mice, as double mutants produce embryos that are phenotypically closer to wild type than inactivation of either complex (12–14). Through their action on gene transcription, COMPASS and PRC1/2 contribute to maintaining developmental decisions during lineage commitment (8–11).

PcG and COMPASS genes frequently harbor inactivating mutations in cancers, suggesting that in certain contexts, they may function as tumor suppressors (15–17). EZH2 is also often overexpressed in other tumorigenic contexts, showing a tumor-specific oncogenic activity. Consequently, EZH2 inhibitors are currently being assessed in several therapeutic protocols (18). Although the function of COMPASS and PRC2 complexes during development is now relatively well described, the mechanisms by which inactivation of these genes contributes to cancer initiation or progression remain much less understood (19). In particular, little is known about how inactivation of the distinct H3K4 and H3K27 methyltransferases and their associated complexes impairs the unfolding of the developmental programs that shape cellular heterogeneity in tumors.

Drosophila is a powerful model organism to investigate the fundamental principles of cancer. In particular, aggressive hierarchical tumors can be induced in the fly developing central nervous system (CNS) originating from neural stem cells, called neuroblasts (NBs) (4, 20, 21). During normal development, NBs divide asymmetrically to self-renew while budding off intermediate progenitors called ganglion mother cells (GMCs). GMCs express the transcription factor Prospero (Pros) that induces the differentiation of two

Aix Marseille University, CNRS, IBDM, Turing Centre for Living systems, Equipe Labellisée Ligue Contre le Cancer, Campus de Luminy Case 907, 13288 Cedex 09 Marseille, France.

*Corresponding author. Email: cedric.maurange@univ-amu.fr

postmitotic neurons or glia after a single GMC division (22). As they divide, NBs progress through a dynamic transcriptional trajectory, known as temporal patterning, that creates various competence windows during embryonic and larval stages (4, 23, 24). Temporal competence windows allow NBs to not only generate different types of neurons or glia at different times but also modulate their proliferative properties as development progresses. Consequently, NBs go through rapid asymmetric divisions during embryogenesis and early larval stages, slower divisions during late larval stages, and undergo a terminal differentiative division during metamorphosis (Fig. 1A) (25–27). Succession of temporal windows in NBs is driven by a cell-intrinsic timing mechanism: a series of sequentially expressed transcription factors, known as temporal transcription factors (tTFs) (Fig. 1A) (25, 28, 29). In the NBs of the ventral nerve cord (VNC), the *Drosophila* equivalent of the vertebrate spinal cord, tTFs temporally delineate three main temporal windows, themselves defined by the expression of various transcription factors and mRNA binding proteins. Highly proliferative NBs in the embryo and early larval stages are characterized by the expression of the two RNA-binding proteins Lin-28 and Insulin-like growth factor 2 mRNA-binding protein (Imp; also known as Igf2bp), and the transcription factor Chinmo. This highly proliferative period can be split into two temporal windows respectively defined by the expression of the sox family transcription factor Dichaete (D) in the embryo and the expression of another transcription factor *grainyhead* (*grh*) in late embryos and early larvae (25). The D-to-Grh switch at the end of embryogenesis is induced by the tTF Castor (Cas) (Fig. 1A) and is necessary for NB self-renewal during larval stages (25, 30, 31). Around mid-larval stages (early L3), the transition to a third temporal

window is triggered by the tTF Seven-up (32–34). Seven-up (orthologous to mammalian COUPTF1/2) switches NBs from an Imp⁺Grh⁺ state to a Syncrip⁺ (Syp) Grh⁺ state. Syp is another RNA binding protein that favors a prodifferentiative state, at least partly via the negative posttranscriptional regulation of the Chinmo/Imp/Lin-28 module (20, 35) and by the activation of the transcription factor Eip93F (E93) (32, 34). The Imp-to-Syp transition terminates the early default self-renewing state conferred by the Chinmo/Imp/Lin-28 module and establishes the competence for differentiation during metamorphosis, such that NBs are absent in adults (Fig. 1A) (26, 36). Descriptions of similar temporal patterning systems are emerging in mammalian neural stem cells, but they remain much less characterized (4, 37–39).

Inactivation of *pros* in NBs leads to GMCs that fail to differentiate into neurons/glia and that instead soon revert to an NB-like state, triggering rapid NB amplification (Fig. 1, B and C) (40–43). *pros* inactivation during early larval stages generates aggressive NB tumors that persist in adults and rapidly kill the fly (32). In *pros*-knockdown tumors, both Imp⁺Chinmo⁺Grh⁺ and Syp⁺E93⁺Grh⁺ tNBs (tumor NBs) are simultaneously observed. This heterogeneity of temporal states reflects the aberrant regulation of the Imp-to-Syp temporal transition (second-to-third competence window) and leads to a hierarchical tumor organization. At the apex of the cellular hierarchy are tNBs expressing *chinmo*, *Imp*, and *lin-28*. In the tumor context, these three genes compose a potent oncogenic module that sustains tNB growth and proliferation and prevents temporal progression, cell cycle exit, and differentiation (32). Clonal studies have demonstrated that Chinmo⁺Imp⁺Lin-28⁺ tNBs constitute CSC-like cells (20). They are required to sustain tumor growth via a default unlimited

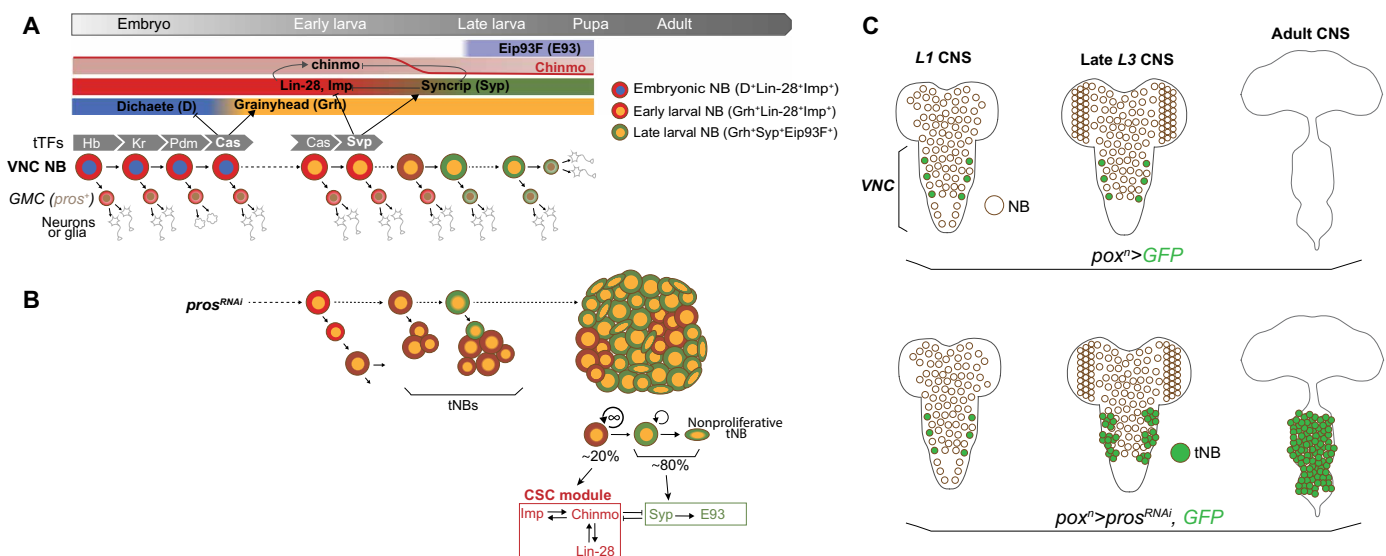


Fig. 1. Temporal patterning in NBs during development and tumorigenesis. (A) Scheme depicting the expression dynamics of temporal patterning in VNC NBs throughout development. NBs undergo terminal differentiation during metamorphosis. tTFs [Hunchback (Hb) → Kruppel (Kr) → Pou-Domain protein 1 (Pdm1) → Castor (Cas) → Seven-up (Svp)] are sequentially expressed in NBs during embryogenesis and early larval development. Cas and Svp promote transitions between three temporal windows: the embryonic D⁺Lin-28⁺Imp⁺ window, the early larval Grh⁺Lin-28⁺Imp⁺ window, and the late larval Grh⁺Syp⁺Eip93F⁺ window. Imp and Syp respectively positively and negatively regulate *chinmo* at the posttranscriptional level, leading to a down-regulation of the Chinmo protein in NBs from mid-larval stages. (B) *pros* knockdown in NBs from early larval stages prevents the differentiation of GMCs, leading to NB tumors that persist growing in adults. Tumorigenic NBs (tNBs) recapitulate part of the larval temporal patterning from mid-to-late larval stages. Coopted larval temporal patterning governs the cellular hierarchy within the tumor. Imp, Chinmo, and Lin-28 define a CSC module in tNBs. tNBs expressing Syp and E93 tend to enter a nonproliferative state. (C) The *pox^n>pros^{RNAi}* system allows the generation of tumors from six NBs of origin located in the VNC. tNBs persist in adults to propagate tumor growth.

proliferative potential and the ability to self-renew. A subset of them, however, stochastically undergoes the Imp-to-Syp transition, and the subsequent Syp⁺E93⁺ tNBs progressively commit toward the end of their proliferation program. Consequently, genetic interventions that block the Imp-to-Syp transition in tumors lead to a higher tumor growth rate (20, 32). Therefore, tumorigenic growth under *pros*-knockdown conditions is due to the combination of the exponential amplification of NBs resulting from the perturbation of the asymmetric division process and sustained proliferation beyond normal developmental stages, due to the aberrant unfolding of the temporal patterning program (4, 20). Orthologs of Imp and Lin28 are also emerging as CSC factors in human (44, 45).

While tTFs schedule the Imp-to-Syp transition in NBs during development, the mechanisms governing the Imp-to-Syp transition in tNBs are unknown. However, the underlying regulation appears robust and finely tuned, as tumors with the same NBs of origin invariably exhibit the same cellular composition with reproducible proportions of Imp⁺ tNBs and Syp⁺ tNBs (Fig. 1B) (20).

In this study, we take advantage of this robust and reproducible hierarchical tumor model and the strong evolutionary conservation of COMPASS and PRC1/2 genes (10, 11) to systematically test how their knockdown affects the growth, cellular composition, and hierarchy of NB tumors. We found that inactivation of *trithorax* (*trx*) (ortholog to MLL1/2) but not of other H3K4 methyltransferases induces a marked amplification of CSC-like cells, leading to an enhanced growth potential. Using single-cell RNA sequencing (scRNA-seq), we demonstrate that this effect largely relies on the larval-to-embryonic reversion of a subset of CSC-like Imp⁺ tNBs that become less likely to undergo the Imp-to-Syp transition and commit toward the end of their proliferation program. We found that in contrast to their developmental antagonism, coinactivation of *trx* and *PRC2* genes synergizes to promote CSC expansion, plasticity, and heterogeneity. This work reveals how inactivation of MLL1/2-COMPASS-like and PRC2 complexes impairs specific developmental programs that govern cellular hierarchies within tumors, therefore promoting cancer progression.

RESULTS

The inactivation of *trx* and *PRC2* genes in NB tumors leads to a “double-edge effect”

We first tested whether *Drosophila* genes of the different COMPASS, PRC1, and PRC2 complexes were sufficient to cause tumorigenesis when inactivated in NBs. Using previously validated UAS-RNAi transgenic lines and the *poxⁿ-GAL4* driver that is active in six lateral NBs in the VNC, we found that inactivation of *PRC1* and *PRC2* genes did not trigger NB amplification and tumorigenesis (fig. S1, A to C), confirming previously published studies (46–49). Similar results were obtained from the RNA interference (RNAi)-mediated inactivation of each of the three H3K4 methyltransferases, *Set1*, *trx*, and *trithorax-related* (*trr*), respective orthologs of *SET1*, *MLL1/2*, and *MLL3/4* (fig. S1, D to F) (10, 48, 50). These results show and confirm that Pcg and COMPASS complexes are not necessary for the NB-to-neuron differentiation process. Thus, unlike for other *Drosophila* tissues (51–53), inactivation of Pcg and COMPASS genes in *Drosophila* neural stem cells is not sufficient to initiate tumorigenesis in the developing CNS.

If inactivation of these genes is not sufficient to initiate tumorigenesis in the CNS, we asked how it could contribute to tumor

evolution in the context of a preestablished NB tumor. For this purpose, we used the previously described *poxⁿ>pros^{RNAi}* system (*poxⁿ-GAL4*, *UAS-dicer2*, *UAS-pros^{RNAi}*, *UAS-GFP*) (Fig. 1C) that allows the systematic generation of green fluorescent protein-positive (GFP⁺) tumors from the same NBs of origin (fig. S1G) (20, 32). RNAi-mediated inactivation of *pros* is induced from early larval stages, leading to NB amplification in late L3 larvae (fig. S1G), and tumors that persist growing in adults (Fig. 1D), ultimately killing the fly 10 to 12 days after eclosion (20). These tumors exhibit reproducible growth characteristics and cellular composition in adult flies, being typically composed of about 10 to 20% of CSC-like Imp⁺Chinmo⁺Lin28⁺ tNBs (thereafter referred to as Imp⁺ tNBs) (Fig. 1B). The rest of tNBs are colabeled with Syp and E93 (thereafter referred to as Syp⁺ tNBs) and endowed with limited self-renewal (20).

Representative genes of the PRC1, PRC2, and of the three COMPASS complexes were knocked down by misexpression of RNAi transgenes in *poxⁿ>pros^{RNAi}* tumors [e.g., *poxⁿ>pros^{RNAi}*, *E(z)^{RNAi}* referred to as *E(z)^{RNAi}* tumors]. The total tumor volume in 6-day-old adults was measured by labeling all tNBs using an anti-Miranda (Mira) antibody (Fig. 2, A and B). The population of Imp⁺ tNBs was assessed by immunostainings against Imp (Fig. 1D). We also used a reporter transgene (*UAS-mCherry^{chinmoUTR}*) that we have previously shown to reflect Chinmo expression in tumors and is therefore specifically expressed in Imp⁺ tNBs (fig. S2) (20, 54). The fraction of Imp⁺ tNBs was calculated as the ratio between the volume delineated by Imp or mCherry immunostaining and the volume delineated by Mira immunostaining labeling all tNBs. Using Imp or mCherry led to similar quantification outcomes (fig. S2A). Tumor volume and the fraction of Imp⁺ tNBs (shown as a percentage) were compared with *control* *poxⁿ>pros^{RNAi}* tumors as a proxy of tumor progression and cellular heterogeneity (Fig. 2, B and C).

Knockdown of PRC1 members did not lead to significant changes in tumor volume and in the proportion of Imp⁺ tNBs compared to *control* tumors (Fig. 2, B and C, and fig. S2B). In contrast, inactivation of PRC2 genes led to tumors that tended to be smaller (except for the *esc^{RNAi}* condition) but that contained a higher proportion of Imp⁺ tNBs (about twice the amount found in *control* *poxⁿ>pros^{RNAi}* tumors) (Fig. 2, A to C, and fig. S2C). These tumors still contained proliferating tNBs as shown with the mitotic marker phospho-Histone 3 (PH3) (Fig. 2A). We validated the specificity of this PRC2-knockdown effect with the misexpression of a second RNAi transgene for each gene and a mutated form of the histone H3 in which the substitution of the lysine-27 by a methionine (H3.3K27M) prevents the trimethylation activity of PRC2 (Fig. 2, B and C, and fig. S2D) (55).

Inactivation of the *set1*-COMPASS complex (using *set1^{RNAi}*) and of the *trr*/MLL3/4-COMPASS-like complex (using *trr^{RNAi}*) (Fig. 2, B and C) and *Utx^{RNAi}* (fig. S2A) also led to smaller tumors but with no significant changes in the proportion of Imp⁺ tNBs. In contrast, the size of *trx^{RNAi}* tumors did not significantly differ from *control* in 6-day-old adults. However, the population of Imp⁺ tNBs underwent an approximate fourfold increase compared to *control* *poxⁿ>pros^{RNAi}* tumors, reaching more than 50% of the total tumor volume (Fig. 2, A to C, and fig. S2, A and E). This *trx*-specific effect was reproduced with two different RNAi transgenes targeting different regions. Thus, these experiments revealed that inactivation of genes of the PRC2 and *trx*/MLL1/2-COMPASS-like complexes significantly alters the composition of *pros^{RNAi}*-mediated NB tumors and leads to an increase in the proportion of Imp⁺ tNBs that are known to exhibit CSC characteristics.

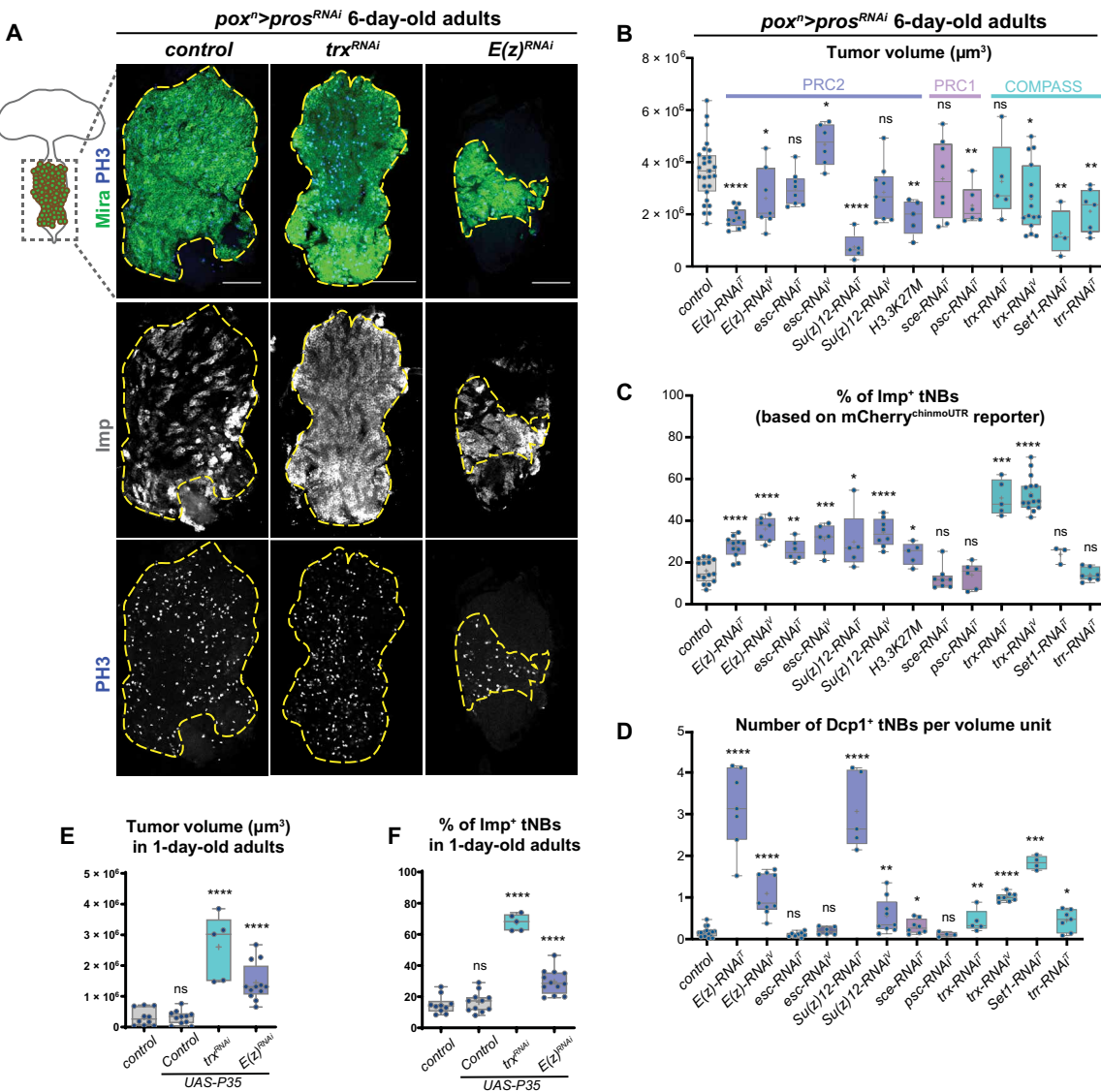


Fig. 2. Knockdown of COMPASS and Polycomb-Group genes in *poxⁿ>pros^{RNAi}* NB tumors. (A) Control *poxⁿ>pros^{RNAi}* tumors or *poxⁿ>pros^{RNAi}* tumors with RNAi-mediated inactivation of *E(z)* and *trx*. Immunostainings against Mira (green) label all tNBs. Immunostainings against Imp (red) label the subpopulation of Imp⁺ tNBs. Immunostaining against PH3 (phosphorylated Histone 3) labels mitotic cells. Scale bars, 100 μm . The dashed lines delimit the area of the tumor in the VNC of 6-day-old adults. Images are single confocal sections. (B to D) Box plots recapitulating quantifications of tumor volumes, proportions of Imp⁺ tNBs, and the number of apoptotic cells for *poxⁿ>pros^{RNAi}* control tumors compared to *poxⁿ>pros^{RNAi}* tumors with the additional RNAi-mediated knockdown of various members of the Pcg and COMPASS complexes. Asterisks above plots indicate statistically significant *P* values for assessing difference with *control* tumors. All measurements are made in tumors that persist in 6-day-old adults. In (C), Imp⁺ tNBs are identified using the mCherry^{chinmoUTR} reporter construct (see also fig. S2). In (D), apoptotic cells are labeled with an anti-Dcp1 antibody. Apoptotic cells are quantified per unit of volume (1 unit = 10,000 μm^3). T in uppercase indicates RNAi lines from the Transgenic RNAi Project (TRIP) provided by the Bloomington Stock Center, while V in uppercase indicates RNAi lines from the Vienna Drosophila Resource Center (VDRC). (E and F) Box plots indicating tumor volumes (E) and the proportions of Imp⁺ tNBs (F) for *poxⁿ>pros^{RNAi}* control tumors compared to *poxⁿ>pros^{RNAi}, p35; *poxⁿ>pros^{RNAi}, p35, *trx^{RNAi}*; and *poxⁿ>pros^{RNAi}, p35, *E(z)^{RNAi}* tumors in the VNC of 1-day-old adults. ns, not significant.***

We had previously shown that an increased proportion of Imp⁺ tNBs systematically leads to a higher tumor growth rate (20). Consistently, immunostaining against PH3 showed that under all conditions, Imp⁺ tNBs exhibit a higher mitotic index than Imp⁻ tNBs, suggesting that Imp⁺ tNBs drive tumor growth in *E(z)^{RNAi}* and *trx^{RNAi}* tumors, too (fig. S2F). Unexpectedly, *trx^{RNAi}* and *PRC2^{RNAi}* tumors that are enriched in Imp⁺ tNBs did not surpass the size of *control* tumors in 6-day-old adults. Staining against the effector Death

caspase-1 (Dcp-1) indicated that apoptosis significantly increases under both the *PRC2^{RNAi}* and *trx^{RNAi}* conditions (Fig. 2D). Blocking apoptosis in the *control*, *trx^{RNAi}*, and *E(z)^{RNAi}* tumors by misexpressing the antiapoptotic viral protein p35 led to the overgrowth of the *trx^{RNAi}* and *E(z)^{RNAi}* tumors but not of the *control* tumors in adults (Fig. 2E and fig. S2G). This is consistent with the lower number of Dcp-1⁺ cells observed under the latter condition. This shows that enhanced apoptosis is at least partly responsible for the lower-than-expected

growth of *PRC2^{RNAi}* and *trx^{RNAi}* tumors. Note that coexpression of p35 and *E(z)^{RNAi}* or *trx^{RNAi}* in NBs during larval development did not cause NB tumors (fig. S1, H to J). Moreover, blocking apoptosis in tumors did not change the proportions of *Imp⁺* tNBs that remained enriched under the *trx^{RNAi}* and *E(z)^{RNAi}* conditions to similar levels (Fig. 2F and fig. S2G). Thus, the enrichment of *Imp⁺* tNBs under *trx^{RNAi}* and *E(z)^{RNAi}* conditions is not due to the preferential apoptosis of *Syp⁺* tNBs. We conclude that knockdown of *PRC2* members and *trx* in a preexisting *pros^{RNAi}* tumor leads to a double-edge effect, where increased apoptosis masks an enhanced growth potential driven by the amplification of *Imp⁺* tNBs. Moreover, these results indicate that increased apoptosis and enrichment of *Imp⁺* tNBs are uncoupled.

Coinactivation of *trx* and *E(z)* synergizes to trigger tumor overgrowth

Together with the COMPASS complexes, the SWI/SNF complex belongs to the larger trithorax-Group (TrxG) proteins. The antagonistic activities of TrxG and Pcg genes were initially demonstrated by the ability of TrxG mutants to suppress Pcg mutant phenotypes during *Drosophila* development (56–58). The antagonistic interactions of Pcg and TrxG genes have also been described in mammalian embryonic stem cells (59) or in tumorigenic contexts. In mice and human tumor models, EZH2 inactivation blocks tumor formation induced by the inactivation of SNF5/SMARCB1, a subunit of the SWI/SNF complex, or MLL3 (60, 61). We wondered whether coinactivation of *E(z)*, the fly ortholog of EZH2, and *trx* in *pox^{n>pros^{RNAi}}* tumors could also suppress the expansion of *Imp⁺* tNBs caused by the single inactivation of either gene. First, to confirm that RNAi-mediated coinactivation of *E(z)* and *trx* could antagonize during development, we inactivated the two genes in wing imaginal discs. Consistently, the ectopic expression of the *Hox* gene *Ultrabithorax* (*Ubx*) observed upon inactivation of *E(z)* was suppressed by coinactivating *trx* (fig. S3). Thus, RNAi-mediated knockdown of Pcg and TrxG genes recapitulates previous antagonistic observations obtained with loss-of-function alleles during development (57). Moreover, coinactivation of *E(z)* and *trx* in NBs was not sufficient to cause tumorigenesis (fig. S1K). Unexpectedly, coinactivation of *E(z)* and *trx* in *pox^{n>pros^{RNAi}}* tumors did not antagonize. While inactivation of either gene in *pox^{n>pros^{RNAi}}* tumors tends to reduce the growth rate due to increased apoptosis, the concomitant knockdown of both genes [*pox^{n>pros^{RNAi}}*, *E(z)^{RNAi}*, *trx^{RNAi}*] tumors, from here on referred to as *E(z)^{RNAi}trx^{RNAi}* tumors] led to a markedly increased growth rate compared to *pox^{n>pros^{RNAi}}* control tumors (Fig. 3, A and B). *E(z)^{RNAi}trx^{RNAi}* tumors exhibited reduced tNB apoptosis compared to *E(z)^{RNAi}* or *trx^{RNAi}* tumors (Fig. 3C), accompanied by a strong enrichment of *Imp⁺* tNBs (76.2 ± 5.5% of the total tumor volume), surpassing the enrichment observed under any single-knockdown conditions (Fig. 3, A and D). These effects could be reproduced when combining *E(z)^{RNAi}* and *trx^{RNAi}* transgenes from different sources (Fig. 3, B and D) or the knockdown of *trx* and *Su(z)12*, another core member of the PRC2 complex (fig. S4). Suppression, under the double-knockdown condition, of the apoptotic phenotype observed under single-knockdown conditions is in accordance with the classical view of antagonistic genetic interactions between Pcg and TrxG genes. In contrast, the exacerbated increase in the population of *Imp⁺* tNBs in *E(z)^{RNAi}trx^{RNAi}* tumors suggests the existence of more complex mechanisms. In conclusion, our data show that coinactivation of *trx* and *PRC2* genes in tumors synergizes to boost tumor growth and amplify the population of *Imp⁺* tNBs.

scRNA-seq of tumors reveals transcriptional trajectories governed by temporal patterning under all conditions

To decipher the molecular mechanisms by which the inactivation of *PRC2* and *trx* genes, alone or in combination, regulates the cellular composition of tumors and affects their growth, we performed scRNA-seq. We sequenced four conditions: the *control* tumors (*pox^{n>pros^{RNAi}}*) (20) and the three perturbed tumors: *E(z)^{RNAi}[pox^{n>pros^{RNAi}, E(z)^{RNAi}]}*, *trx^{RNAi}[pox^{n>pros^{RNAi}, trx^{RNAi}]}*, and *E(z)^{RNAi}trx^{RNAi}[pox^{n>pros^{RNAi}, E(z)^{RNAi}, trx^{RNAi}]}*.

We dissected and dissociated tumors that persist in adults and proceeded to fluorescence-activated cell sorting (FACS) of GFP⁺ tumor cells. We analyzed the transcriptomes of cells isolated from each type of tumors using the Seurat R package (62). Cells were distributed according to their transcriptomic similarities on Uniform Manifold Approximation and Projection (UMAP) plots for graphical visualization. tNBs were identified by the expression of NB identity genes such as *miranda* (*mira*) (fig. S5). When analyzing all conditions independently, we found that for all of them, the bulk of tNBs were grouped in a large single cluster that could be subdivided in subclusters according to the chosen resolution. All conditions also included smaller outlying clusters. The latter were characterized by expression of the neuronal marker *elav*, indicating differentiating neurons, or by the stress sensor gene *Growth arrest and DNA damage-inducible 45* (*Gadd45*) (fig. S5). *Gadd45* is a well-described tumor suppressor gene known to promote cell cycle arrest and apoptosis (63). The fraction of *Gadd45⁺* clusters was particularly prominent under the *E(z)^{RNAi}* condition that contained five clusters (3, 8, 9, 10, and 11 and 12, encompassing 23% of the cells) expressing consistent levels of the gene (fig. S5). In contrast, the *Gadd45⁺* clusters represented 7% of the cells under the *control* condition and about 1% under the *trx^{RNAi}* and *E(z)^{RNAi}trx^{RNAi}* conditions (fig. S5). These data are consistent with the high apoptotic and reduced growth rate of *E(z)^{RNAi}* tumors, whereas the very low levels under the *trx^{RNAi}* and *E(z)^{RNAi}trx^{RNAi}* conditions are consistent with *trx* inhibition leading to a repression of the *Gadd45*-dependent stress pathway. Thus, inactivation of *trx* may favor tumor growth by inhibiting *Gadd45*. No glia (*repo⁺*) were detected.

We then investigated whether the enrichment of *Imp⁺* tNBs observed by immunostaining upon down-regulation of *E(z)* and/or *trx* was also detected at the RNA level. For this purpose, all conditions were computationally merged. Notably, the sequencing data confirmed that *E(z)* and *trx* RNAs were down-regulated appropriately upon RNAi (Fig. 4A). In agreement with immunostainings, the early temporal gene *Imp* was enriched under the three perturbed conditions compared to the *control* condition, while the late temporal marker *E93* was strongly reduced. Differential analysis confirmed that *Imp* and *E93* are among the most differentially expressed genes when comparing perturbed tumors to *control* tumors (data S1). Together, these analyses confirm the good quality of our single-cell data.

We then investigated potential transcriptional trajectories within tNBs for each tumor condition using Monocle 3 (64). The *Gadd45⁺* clusters were computationally excluded as they likely constitute unfit tNBs. We also excluded the *elav⁺* neuronal cluster to focus on proliferating cells. For all conditions, we observed opposing gradients of *Imp* and *E93*, respectively, along the computed trajectories/pseudotime (Fig. 4B). This indicates that tNBs under each tumor condition progress along a transcriptional trajectory that is shaped by temporal patterning and that tNBs with high levels of *Imp* are

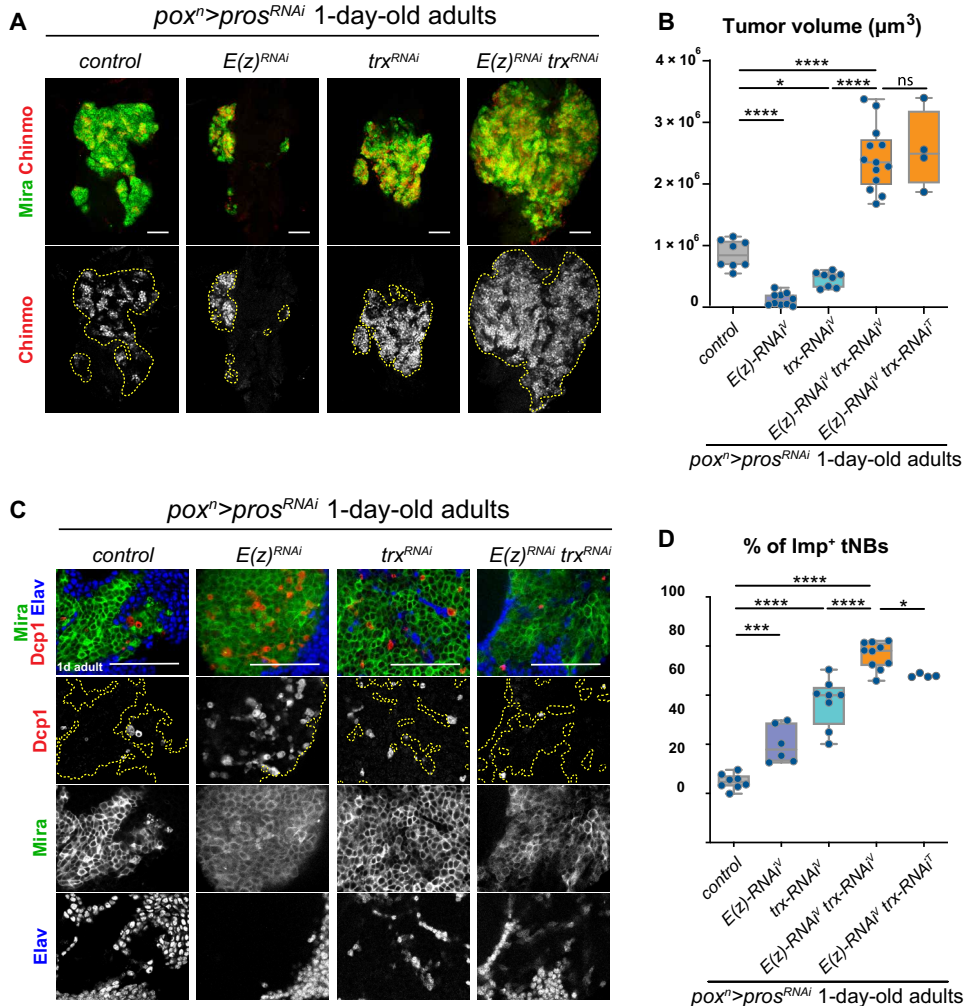


Fig. 3. Coinactivation of PRC2 genes and *trx* acts synergistically to increase the proportion of Imp⁺ tNBs and amplify tumor growth. (A) Control *poxⁿ>pros^{RNAi}* tumors or *poxⁿ>pros^{RNAi}* tumors with RNAi-mediated inactivation of *E(z)* or *trx* or coinactivation of *trx* and *E(z)*. Immunostainings against Mira (green) label all tNBs. Immunostainings against Chinmo (red) label the subpopulation of Imp⁺ tNBs. The dashed lines delimit the area of the tumor in the VNC of 1-day-old adults. Images are single confocal sections. Scale bars, 50 μm . (B) Box plots recapitulating quantifications of tumor volumes (in cubic micrometers) for the genotypes indicated in (A). Tumor volume measurements are made on the basis of anti-Mira immunostaining. T in uppercase indicates RNAi lines from the TRIP provided by the Bloomington Stock Center, while V in uppercase indicates RNAi lines from the VDRC. (C) Immunostainings of tumors showing apoptotic cells with anti-Dcp1 antibody. Apoptosis is strongly reduced upon coinactivation of *E(z)* and *trx* compared to the single inactivation of *E(z)* or *trx*. Scale bars, 50 μm . Images are single confocal sections. (D) Box plots recapitulating quantifications of proportions of Imp⁺ tNBs for the genotypes indicated in (A). Imp⁺ tNBs are identified with an anti-Chinmo antibody. All measurements are made in tumors that persist in the VNCs of 1-day-old adults.

positioned at the root of the trajectory. By analogy with the *control* condition (20), this strongly suggests that Imp⁺ tNBs also behave as CSCs under the perturbed conditions.

The double-edge effect upon inactivation of PRC2 genes is caused by concomitant up-regulation of *Hox* genes and *lin-28*

We then investigated further the genes that were differentially expressed between *E(z)^{RNAi}* and *control* tumors. In addition to *Gadd45*, the posterior *Hox* genes *abd-A* and *Abd-B* as well as *lin-28* appeared among the most highly up-regulated genes in *E(z)^{RNAi}* tumors (Fig. 5A and data S1). Previous studies have shown that the inactivation of PRC1/2 genes causes derepression of posterior *Hox* genes in larval thoracic NBs, leading to their death by apoptosis (47, 65).

We confirmed by immunostaining that *abd-A* is indeed strongly derepressed in *E(z)^{RNAi}* tumors (Fig. 5B). Misexpression of *abd-A* in *poxⁿ>pros^{RNAi}*, *UAS-abd-A* flies resulted in an absence of NB tumors in larvae. Inhibition of apoptosis in this context (*poxⁿ>pros^{RNAi}*, *UAS-abd-A*, *UAS-p35*) fully restored tumor growth (Fig. 5C). Together, these data indicate that apoptosis in PRC2^{KD} tumors is at least partially due to *abd-A* derepression.

Notably, the derepression of *Hox* genes observed in *E(z)^{RNAi}* tumors was completely rescued in *E(z)^{RNAi} trx^{RNAi}* tumors (Fig. 5, A to C), which do not exhibit extensive apoptosis. Thus, *trx* inactivation can antagonize the derepression of *abd-A* and *Abd-B* caused by *E(z)* inactivation. This is consistent with *Hox* genes being canonical targets of PcG and TrxG proteins during development and tumorigenesis.

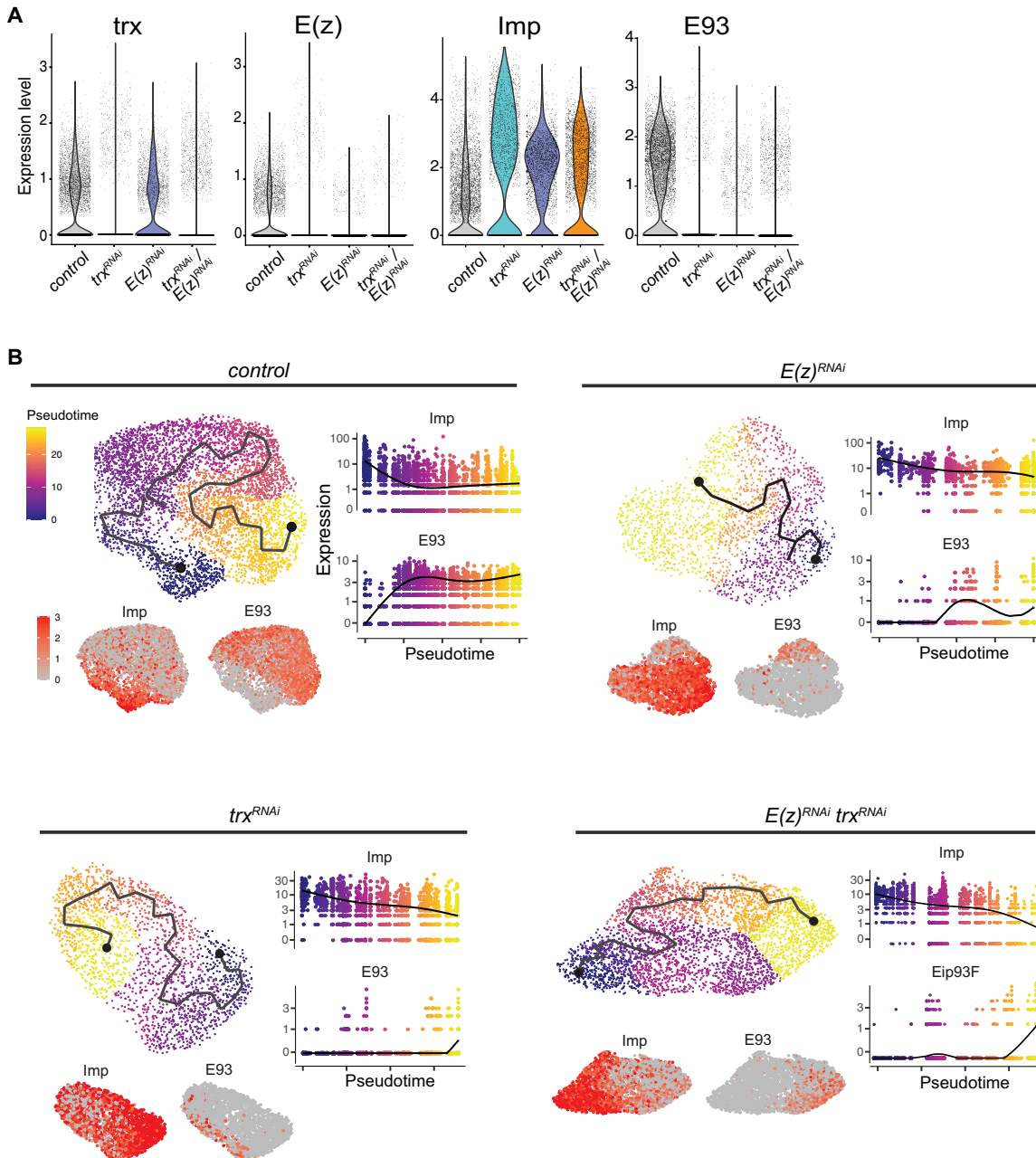


Fig. 4. Expression of Imp and E93 in tumors at the single-cell level. (A) Violin plots depicting expression levels of representative genes under different tumor conditions from scRNA-seq data. (B) Trajectory and pseudotime analyses using tNBs for each tumor condition using Monocle 3. Imp and E93 are expressed in an anticorrelative manner along pseudotimes consistent with a common temporal patterning-mediated differentiation trajectory for all conditions.

In line with scRNA-seq data, immunostainings against Lin-28 revealed global derepression across tNB populations in $E(z)^{RNAi}$ tumors (Fig. 5D). This effect was also observed in tumors lacking $Su(z)12$, indicating a phenotype common to the inactivation of PRC2 genes (Fig. 5D). However, in contrast to *Hox* genes, *lin-28* up-regulation was not suppressed under the $E(z)^{RNAi} \& trx^{RNAi}$ condition (Fig. 5A), although *lin-28* up-regulation was not observed in trx^{RNAi} tumors (Fig. 5, A and D, and data S1). Thus, the regulation of *lin-28* in tumors does not follow the canonical regulation by Pcg and TrxG proteins observed for *Hox* genes. We had previously

demonstrated that *lin-28* in NB tumors forms a positive feedback loop with Chinmo and Imp (32). Thus, *lin-28* derepression in the $E(z)^{RNAi}$ tumors likely favors the CSC state by reinforcing the Chinmo/Imp/Lin-28 feedback loop. Knockdown of *lin-28* in the $E(z)^{RNAi}$ tumors could not be achieved to formally test this hypothesis as the use of available RNAi lines did not lead to efficient Lin-28 down-regulation.

In conclusion, single-cell analysis unveils a mechanism that could account for the observed “double-edge effect” upon inactivation of *E(z)*: Derepression of *Hox* genes (possibly via or in parallel to

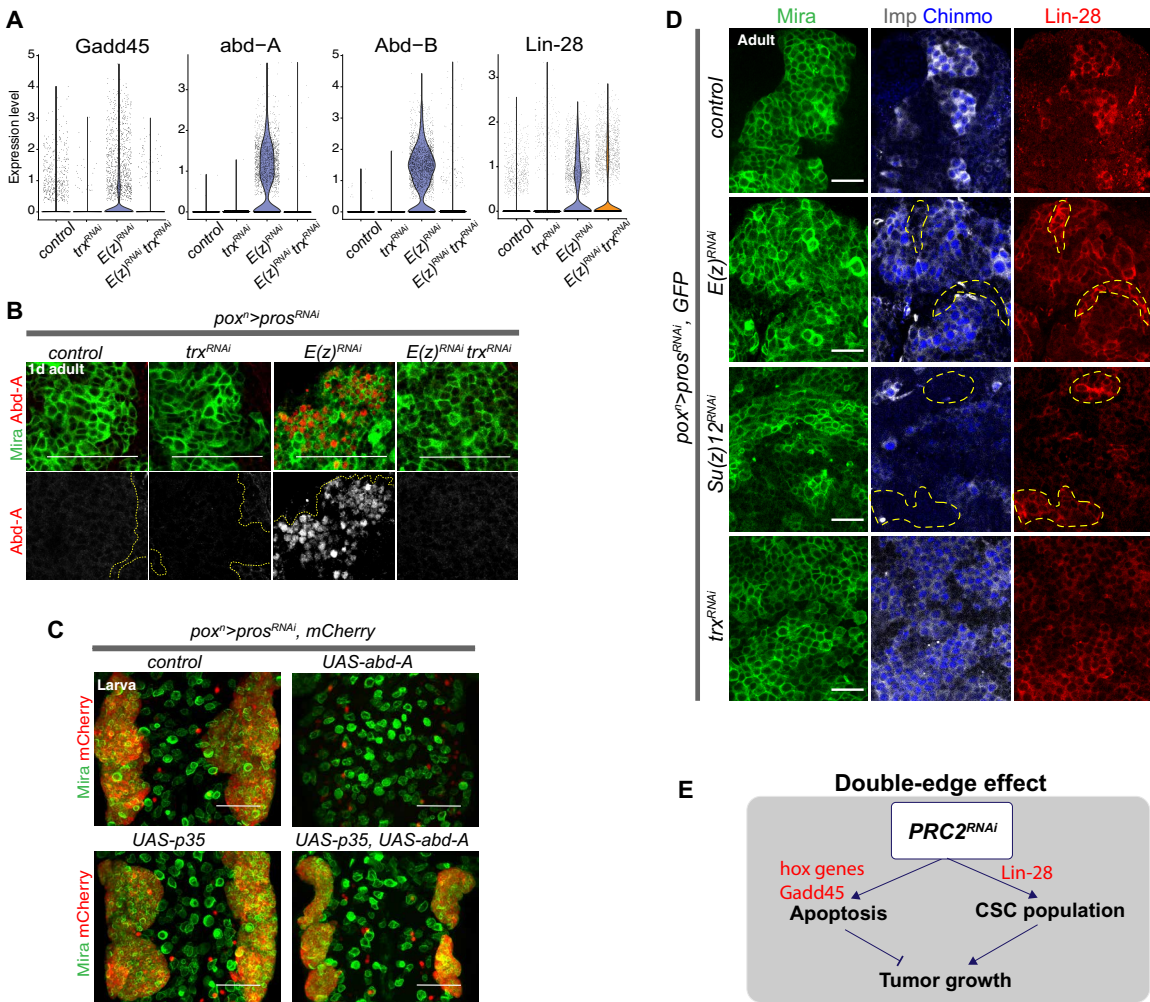


Fig. 5. PRC2 inactivation causes derepression of Hox genes and *lin-28*. (A) Violin plots comparing expression levels of various genes for all conditions. (B) Anti-Abd-A immunostainings in tumors of the different genotypes. Tumors are from 1-day-old adults, and tNBs are marked with anti-Mira. (C) Overexpression of *abd-A* in $pox^n>pros^{RNAi}$ larvae prevents tumor induction. Tumors are restored when apoptosis is blocked by the caspase inhibitor p35 despite *abd-A* overexpression. Both wild-type NBs and tNBs are labeled with anti-Mira antibody (green), whereas tumor cells are identified by their expression of the NLS:mCherry (red). (D) Immunostainings in adult tumors of the different genotypes. tNBs are marked with anti-Mira. Imp⁺ tNBs are marked with anti-Imp and anti-Chinmo. In *control* tumors, immunostainings against Lin-28 show that Lin-28 is coexpressed with Imp and Chinmo in tNBs. In contrast, Lin-28 is ectopically expressed in some tNBs in the absence of Chinmo and Imp upon inactivation of *E(z)* or *Su(z)12* (delineated by yellow dotted lines). (E) Scheme summarizing a model for the double-edge effect induced by the inactivation of PRC2 genes. Scale bars, 50 μ m. Images are single confocal sections except for (C) representing a projection of several sections.

Gadd45) enhances apoptosis, while concomitant derepression of oncogenes such as *lin-28* could favor CSC amplification (Fig. 5E). In addition, while the derepression of canonical Pcg/TrxG targets such as *Hox* genes is suppressed in $E(z)^{RNAi} trx^{RNAi}$ tumors, *lin-28* is maintained at high levels. Consequently, in the absence of significant apoptosis, $E(z)^{RNAi} trx^{RNAi}$ tumors can unleash their growth potential driven by the enriched population of Imp⁺ tNBs.

The temporal patterning gene regulatory network is a privileged target of the COMPASS and PRC2 complexes in tumors

To further elucidate the mechanisms causing the enrichment of Imp⁺ CSC-like tNBs under the perturbed tumor conditions, we focused on the genes that were differentially expressed in the population of Imp⁺ tNBs. Using Seurat R package (62), we computationally

isolated for each condition the populations of Imp⁺ tNBs by selecting the clusters encompassing most Imp⁺ E93⁻ tNBs (clusters highlighted in red in fig. S5). Then, the selected population of Imp⁺ tNBs for the three perturbed conditions was respectively compared to the population of Imp⁺ tNBs of the *control* condition to identify differentially expressed genes (data S2).

Reactome pathway analysis of the differentially expressed genes indicated that the respiratory electron transport genes of mitochondria are up-regulated in Imp⁺ tNBs of the trx^{RNAi} and $E(z)^{RNAi} trx^{RNAi}$ conditions compared to *control* Imp⁺ tNBs (Fig. 6A). These data suggest that loss of *trx* enhances mitochondrial metabolism, which is consistent with the hypothesis that high levels of oxidative phosphorylation promote CSC activity (20, 66, 67). No up-regulated pathway could be identified by gene ontology analysis under the $E(z)^{RNAi}$ condition compared to *control*.

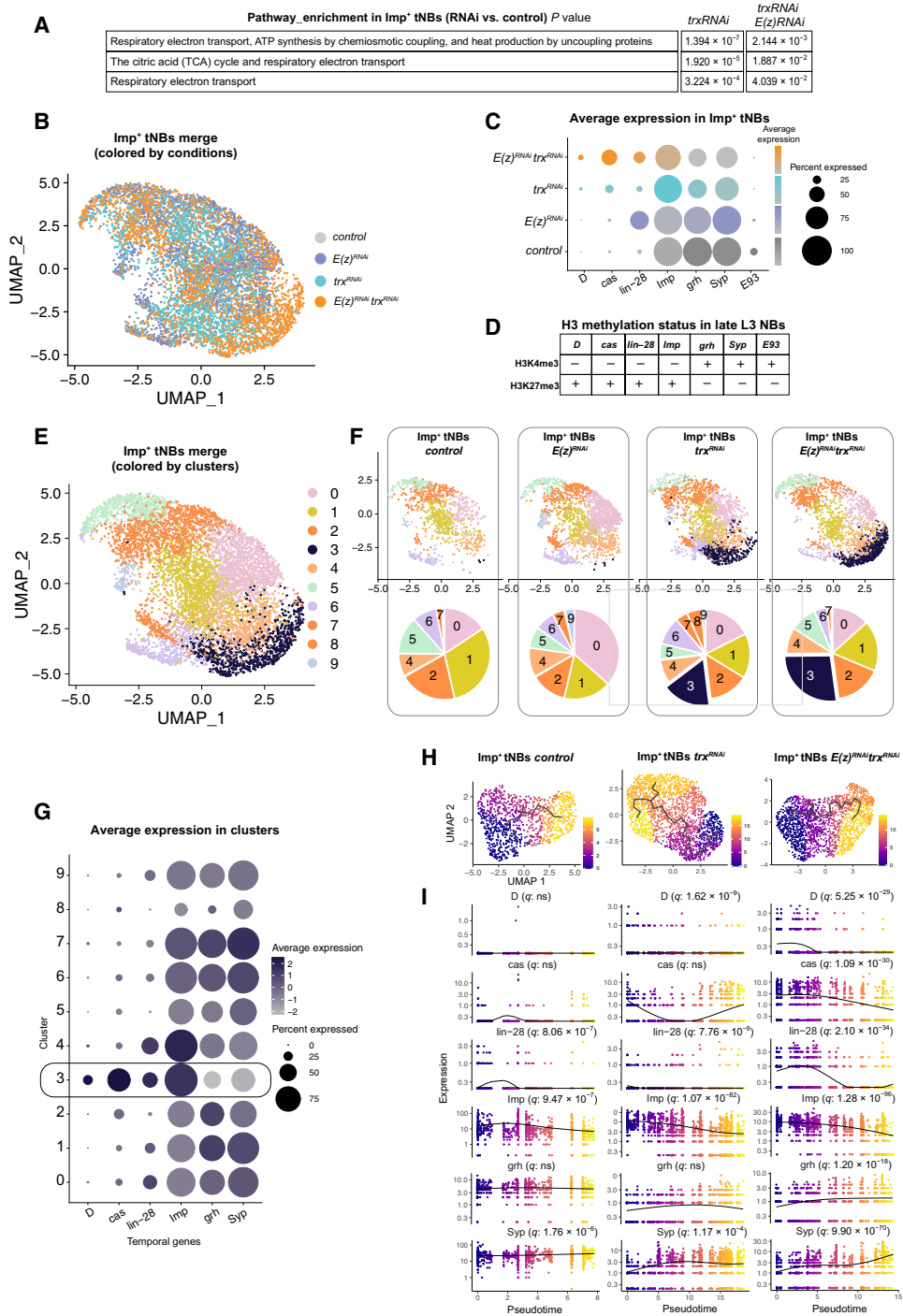


Fig. 6. Identification by scRNA-seq of an embryonic-like tNB subpopulation in tumors upon inactivation of *trx*. (A) Pathway enrichment in the Imp⁺ tNB population of *poxⁿ>pros^{RNAi}*, *trx^{RNAi}* and *poxⁿ>pros^{RNAi}, E(z)^{RNAi}* tumors compared to the Imp⁺ tNB population of control *poxⁿ>pros^{RNAi}*. (B) UMAP representation of the merged populations of Imp⁺ tNBs from the control and perturbed conditions. Dots are colored according to the genotype of tumors. (C) Dot plot depicting the average expression of temporal identity markers (from scRNA-seq data) in the Imp⁺ tNB population according to tumor genotype. (D) Summary of fig. S6 depicting the histone H3 methylation state in late L3 NBs. (E) UMAP representation of the merged populations of Imp⁺ tNBs from the control and perturbed conditions. Dots are colored according to clusters of transcriptional similarities. (F) Distribution of cells for each tumor genotype in the UMAP representation depicted in (E). Pie charts show the proportions of cells within each cluster for the depicted genotype. (G) Dot plot showing the average expression of temporal identity markers for the 10 clusters depicted in the UMAP representation in (E). Cluster 3 is enriched in embryonic temporal markers. (H) Inferred transcriptional trajectories (black line) within the population of Imp⁺ tNBs of the control, *poxⁿ>pros^{RNAi}*, *trx^{RNAi}*, and *poxⁿ>pros^{RNAi}, E(z)^{RNAi}* tumors. Dots are colored as a function of pseudotime. (I) Plots showing the dynamics of expression of temporal genes as a function of pseudotime for the three above conditions. *q* values represent adjusted false discovery rates, indicating that temporal genes significantly vary as a function of pseudotime.

We also noticed that many but often distinct members of the larval temporal patterning system were deregulated in *E(z)^{RNAi}* and *trx^{RNAi}* tumors (data S2). Then, using Seurat R packages (62), we computationally merged the populations of Imp⁺ tNBs from the control and perturbed conditions (Fig. 6B) and compared the expression of temporal patterning genes for each condition. As expected, the level of the early embryonic/larval temporal gene *lin-28* was particularly high in the population of Imp⁺ tNBs of *E(z)^{RNAi}* tumors (Fig. 6C and data S2). More generally, our data show a global up-regulation of embryonic temporal identity genes (*D*, *cas*, *lin-28*, and *Imp*) and a global down-regulation of larval temporal identity genes (*grh*, *Syp*, and *E93*) in the Imp⁺ tNBs of perturbed tumor conditions compared to *control* tumors (Fig. 6C and data S2). This trend is particularly strong under the *trx^{RNAi}* and *E(z)^{RNAi} trx^{RNAi}* conditions. Therefore, unlike for *Hox* genes, deregulation of temporal genes is exacerbated in the Imp⁺ tNBs of *E(z)^{RNAi} trx^{RNAi}* tumors (Fig. 6C). Thus, temporal patterning genes emerge as being among the most significantly and consistently deregulated gene network in NB tumors lacking *PRC2* or *trx* genes.

To investigate whether these temporal patterning genes are direct targets of PRC2 and COMPASS complexes in NBs, we interrogated recently published chromatin immunoprecipitation experiments aiming at identifying genes subjected to the repressive H3K27me³ and the permissive H3K4me³ marks in late L3 NBs (46). In *Drosophila*, the H3K4me³ mark is deposited by the Set1-COMPASS and Trx/MLL1/2-COMPASS-like complexes. The data show that all the aforementioned temporal patterning genes exhibit histone methylation marks that correlate with their expression state in late L3 NBs: The repressive H3K27me³ mark is dominant at early temporal genes (*D*, *cas*, *lin-28*, and *Imp*), and the permissive H3K4me³ mark is dominant in late temporal genes (*grh*, *syp*, *Syp*, and *E93*) (Fig. 6D and fig. S6). Consistently, *abd-A* is associated with strong H3K27me³, while *chinmo* retains H3K4me³ mark in line with its continuous transcription in NBs throughout larval stages (54, 68). In conclusion, the chromatin immunoprecipitation data and the scRNA-seq analysis show that the temporal patterning gene network is a privileged target of PRC2 and COMPASS (Set1 and/or Trx) complexes in NBs. Consequently, the temporal network appears to undergo a reconfiguration toward an embryonic-like state in NB tumors upon knockdown of these chromatin complexes.

***trx* inactivation induces a subpopulation of Imp⁺ tNBs with an embryonic-like identity**

We then investigated how the reconfiguration of the temporal gene network under the *E(z)^{RNAi}*, the *trx^{RNAi}*, or the *E(z)^{RNAi} trx^{RNAi}* conditions may affect the cellular heterogeneity within the population of CSC-like Imp⁺ tNBs. The merged populations of Imp⁺ tNBs from the four conditions were partitioned into 10 clusters revealed on a UMAP representation using Seurat (Fig. 6E). To investigate whether all 10 clusters are distributed evenly throughout conditions, we visualized the UMAP distribution of clusters for each condition side by side (Fig. 6F). This shows that Imp⁺ tNBs of the perturbed conditions distribute throughout the seven clusters that encompass all Imp⁺ tNBs present under the *control* condition. However, the UMAP also revealed novel clusters that are more specific to the perturbed conditions, suggesting that *E(z)* or *trx* inactivation increases the cellular heterogeneity within the population of Imp⁺ tNBs (Fig. 6F). Differential analysis of gene expression between the different clusters indicates that cluster 3 (black cluster) emerging

under the *trx^{RNAi}* condition up-regulates *cas* and *D* (data S3). In addition, cluster 3 exhibits a strong down-regulation of *grh* and *Syp* (Fig. 6G and fig. S7). This suggests that cluster 3 may represent an emerging population of tNBs with an embryonic-like temporal identity. This embryonic-like D⁺, cas⁺ grh⁻, Syp⁻ population becomes even more prominent under the *E(z)^{RNAi} trx^{RNAi}* condition (Fig. 6F).

Last, we inferred trajectories and pseudotime within the population of Imp⁺ tNBs for each condition using Monocle 3 (64). Investigating temporal genes that vary as a function of time ($q < 0.05$) revealed a clear D \rightarrow cas \rightarrow grh \rightarrow Syp temporal sequence for the *E(z)^{RNAi} trx^{RNAi}* condition (already emerging under the *trx^{RNAi}* condition). However, this sequence is not detected under the *control* condition with *cas*, *D*, and *grh* not varying along pseudotime (Fig. 6H). Thus, *trx* inactivation triggers a heterogeneity of temporal states in the population of Imp⁺ tNBs by inducing the emergence of an earlier embryonic-like temporal identity in addition to the preexisting larval temporal identity state. Moreover, the embryonic temporal identity state appears reinforced upon the coinactivation of both *E(z)* and *trx*.

Upon *trx* inactivation, embryonic-like tNBs emerge from the temporal reversion of larval-like tNBs

We tested whether our observations at the transcriptomic level were corroborated at the protein level. Immunostainings in adult tumors indicated that subsets of tNBs in *trx^{RNAi}* tumors up-regulate *D* and *Cas*, with a more pronounced up-regulation observed under the *E(z)^{RNAi} trx^{RNAi}* condition (Fig. 7, A and B, and fig. S8, A and B). Similar observations could be made for the down-regulation of *Grh* (Fig. 7, A and B). We noticed that *D* up-regulation generally coincided with *Grh* down-regulation in tNBs and that these tNBs were usually found in small groups dispersed throughout tumors, suggesting that the D⁺Grh⁻ state is relatively stable and can be clonally transmitted (Fig. 7A).

Then, we tested whether similar dysregulation of temporal identity genes could also be observed in larval stages. However, we could not detect any up-regulation of *D* or down-regulation of *Grh* in tNBs from the *trx^{RNAi}* and *E(z)^{RNAi} trx^{RNAi}* conditions in larval tumors (Fig. 7C and fig. S8C). In early L3, the NB of origin can be distinguished in tumors based on its large size and its lateral position. In both types of tumors, it expressed *Grh* but not *D*, showing that the D-to-Grh transition was not blocked (Fig. 7C). Thus, the presence of Grh⁻D⁺ tNBs in the *trx^{RNAi}* and *E(z)^{RNAi} trx^{RNAi}* tumors does not result from a faulty D-to-Grh transition in the NB of origin but gradually emerges from a population of larval-like tNBs and becomes evident in adult tumors. In addition, down-regulating *E(z)* and *trx* in NBs during development does not significantly delay the Imp-to-Syp transition, consistent with an absence of a larval-to-embryonic temporal reversion in the developmental context (fig. S8D). Together, these experiments demonstrate that, in the tumor context, knockdown of *trx* or *trx/E(z)* progressively promotes the reversion from a larval-to-embryonic-like temporal identity in a subset of tNBs, triggering plasticity in the normally rigid developmental hierarchy.

Repression of *grh* prevents the Imp-to-Syp transition and maintains the CSC-like state

To investigate whether the larval-to-embryonic temporal reversion is relevant for the regulation of the CSC-like population of Imp⁺ tNBs in adult tumors, we misexpressed the embryonic temporal identity genes *D* or *cas* in *poxⁿ>pros^{RNAi}* tumors. We observed a significant increase in the proportion of Imp⁺ tNBs in adult tumors

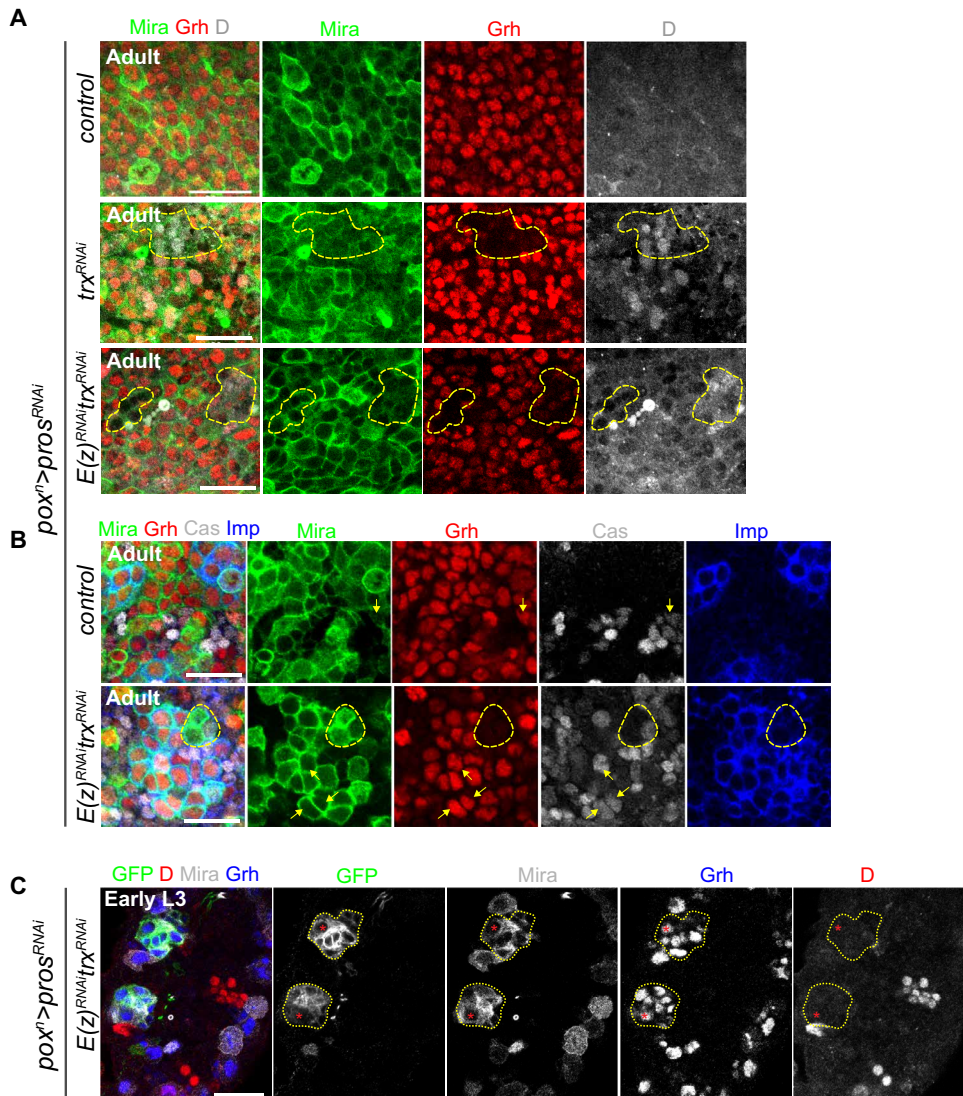


Fig. 7. Up-regulation of Cas and D and down-regulation of Grh are observed in *trx^{RNAi}* or *E(z)^{RNAi} trx^{RNAi}* tumors in adults but not in larvae. (A) Immunostainings against Grh and D in *control* (*pox^n>pros^{RNAi}*), *trx^{RNAi}* (*pox^n>pros^{RNAi}, *trx^{RNAi}*), and *E(z)^{RNAi} trx^{RNAi}* [*pox^n>pros^{RNAi}, *E(z)^{RNAi}, *trx^{RNAi}**] tumors found in the VNCs of adults. tNBs are labeled with anti-Mira. The yellow dashed line delineates a cluster of tNBs down-regulating Grh. (B) Immunostainings against Grh, Cas, and Imp in *control* and *E(z)^{RNAi} trx^{RNAi}* tumors found in the VNCs of adults. Arrows illustrate examples of tNBs (Mira⁺) expressing Cas. The yellow dashed line delineates a cluster of tNBs down-regulating Grh. (C) Immunostainings against Grh and D in early L3 larvae. The yellow dotted lines delineate tNBs of two initiating *E(z)^{RNAi} trx^{RNAi}* tumors. As in normal NBs (Mira⁺ GFP⁻ cells), the D-to-Grh transition operates normally in the tNB at the origin of tumors (red asterisk). Scale bars, 20 μm for all pictures. Images are single confocal sections.**

misexpressing *D* (2.1-fold increase) or *cas* (1.3-fold increase) (Fig. 8A), associated with a significant increase in tumor growth upon *cas* misexpression (Fig. 8B). Thus, ectopic expression of embryonic temporal factors is sufficient to promote expansion of the Imp⁺ tNB population and subsequent tumor overgrowth.

We also inactivated *grh* in *pox^n>pros^{RNAi}* tumors from their initiation in early larvae. *grh* inactivation in tumors led to the ectopic reactivation of *cas*, indicating that *grh* down-regulation is sufficient to cause the reactivation of embryonic temporal factors (Fig. 8C). Notably, in 2- to 5-day-old adults, large tumors were observed that contained up to 94% of Imp⁺ tNBs (representing more than a five-fold increase compared to *control* tumors) (Fig. 8, A and D). This shows that Grh is necessary for the Imp \rightarrow Syp transition to occur in

tumors. Moreover, *grh^{RNAi}* tumors tend to be larger compared to their *control* counterparts in 1-day-old adults, suggesting a possibly higher growth rate (Fig. 8B). Because all Imp⁺ tNBs lack Grh in this context, our results imply that Grh⁻Imp⁺ tNBs can sustain tumor growth and therefore can act as CSCs. In addition, they demonstrate that these embryonic-like tNBs are less likely to progress throughout the temporal trajectory than larval-like Grh⁺Imp⁺ tNBs and therefore tend to remain at the top of the tumor hierarchy.

We found that the growth rate of *trx^{RNAi}* tumors accelerates during adult stages to catch up to the size of *control* tumors despite an initial lower growth rate in larvae (fig. S9A). This growth is fueled by a higher mitotic rate in *trx^{RNAi}* tumors of 6-day-old adults (fig. S9, B and C), showing that temporal reprogramming correlates

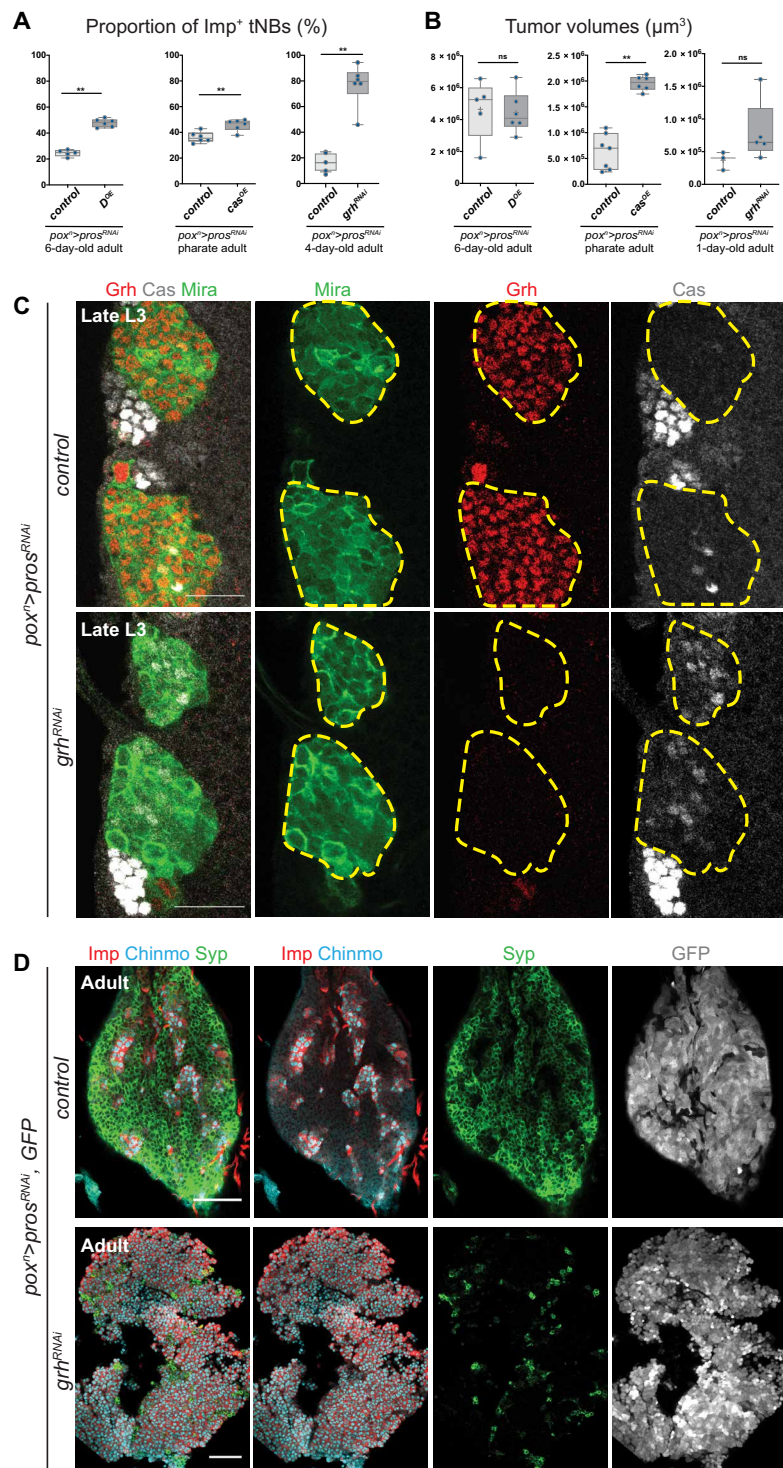


Fig. 8. grh down-regulation promotes cas up-regulation, prevents the Imp-to-Syp transition, and accelerates tumor growth. (A) Box plots recapitulating the effect of cas and D overexpression (OE) or grh knockdown on the proportion of Imp⁺ tNBs. (B) Box plots recapitulating the effect of cas and D misexpression or grh knockdown on tumor growth. (C) Yellow dotted lines delineate *poxⁿ>pros^{RNAi}* and *poxⁿ>pros^{RNAi}, grh^{RNAi}* tumors in a larval VNC. Immunostaining against Cas indicate that Cas is up-regulated in *poxⁿ>pros^{RNAi}*, *grh^{RNAi}* tumors. Scale bars, 20 μm . All images are single confocal sections. (D) Immunostainings against Imp, Chinmo, and Syp in *poxⁿ>pros^{RNAi}* and *poxⁿ>pros^{RNAi}, grh^{RNAi}* tumors found in adult VNCs. GFP labels all tNBs. Scale bars, 50 μm .

with an increased growth potential. In conclusion, our experiments support the idea that the progressive larval-to-embryonic temporal reversion observed in *trx*^{RNAi} and *E(z)*^{RNAi}*trx*^{RNAi} tumors blocks the Imp-to-Syp hierarchical transition, contributing to the expansion of the CSC-like Imp⁺ tNB population that fuels tumor growth.

DISCUSSION

We find that in the *Drosophila* CNS, inactivation of the Trx/MLL1/2-COMPASS-like complex, rather than being a trigger for tumor initiation, promotes progression of preexisting tumors by disrupting the established cellular hierarchy. Moreover, we identify an unexpected synergistic effect of the concomitant inactivation of *trx* and *PRC2* genes. Our study suggests that, by abolishing the epigenetic constraints that guide developmental trajectories at the top of tumor hierarchies, co-knockdown of the Trx/MLL1/2-COMPASS-like and PRC2 complexes can cooperate to induce CSC plasticity and expansion (Fig. 9).

trx inactivation increases CSC heterogeneity via temporal patterning reversion

We had previously demonstrated that *pros*^{RNAi} tumors are composed of tNBs locked in a temporal program spanning early to late larval stages (20). In these tumors, tNBs expressing Imp constitute the pool of tumor-propagating cells, therefore exhibiting CSC-like properties, at the top of a unidirectional tumor hierarchy. Our single-cell transcriptomic analysis now demonstrates that *trx* inactivation progressively induces the emergence of an additional population of Imp⁺ tNBs exhibiting embryonic temporal characteristics, as defined by the reactivation of *D* and *cas* and the repression of *grh*. At least two lines of evidence argue that the new embryonic-like Imp⁺ tNB population can also act as CSCs. First, pseudotime analysis locates this population at one extremity of the tumor differentiation trajectory. This strongly suggests that embryonic-like tNBs are at the top of the tumor hierarchy. Second, the coinactivation of *grh* and *pros* produces tumors that are almost exclusively composed of Imp⁺ tNBs in adults, demonstrating that embryonic-like tNBs can

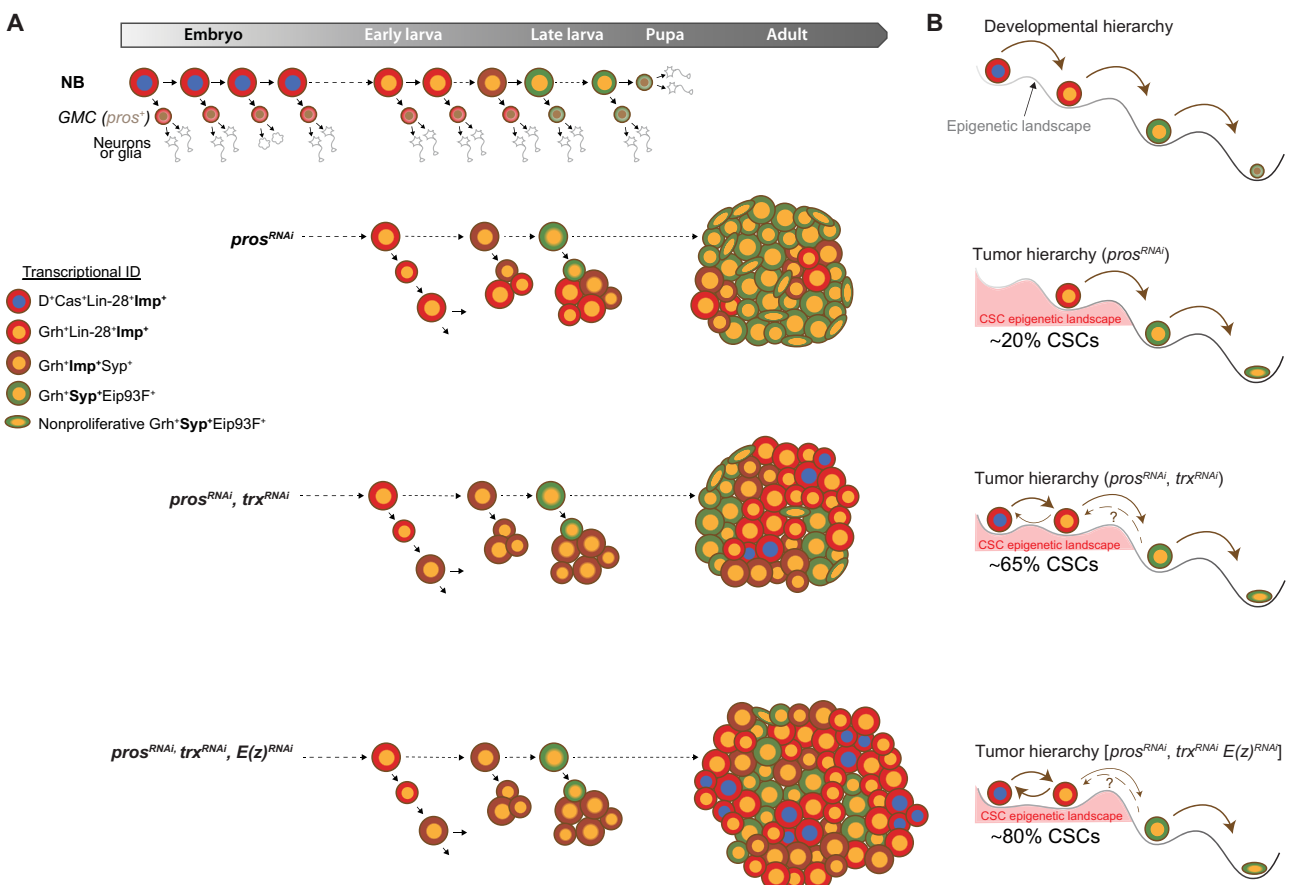


Fig. 9. Knockdown of *trx* and *PRC2* genes impairs temporal progression at the top of the tumor hierarchy. (A) NB tumors induced by the loss of *pros* exhibit a strict hierarchical organization governed by the recapitulation of larval temporal patterning. *trx* inactivation in *pros*^{RNAi} tumors promotes temporal reversion and the appearance of Imp⁺ tNBs with an embryonic temporal identity (*D*⁺*Cas*⁺*Grh*⁻) in adult tumors. The embryonic temporal identity is reinforced upon coinactivation of *trx* and *E(z)*. (B) During development, NBs are subjected to a hierarchy of temporal/developmental states likely partly guided by an epigenetic landscape. During *pros*^{RNAi}-mediated tumorigenesis, larval temporal patterning is coopted and induces a cellular hierarchy. Inactivation of *trx* flattens the epigenetic landscape at the top of the tumor hierarchy. This leads to temporal reversion and emergence of a tNB population with an embryonic-like temporal identity (*D*⁺*Cas*⁺*Grh*⁻) at the top of the hierarchy. Embryonic Imp⁺ tNBs are less inclined to progress toward the late steps of the hierarchy. Flattening of the epigenetic landscape at the top of the hierarchy is worsened by the coinactivation of *PRC2* genes, locking Imp⁺ tNBs into a spectrum of CSC states. Our work suggests that *trx* and *PRC2* genes are essential regulators of the epigenetic landscape guiding temporal progression at the top of the tumor hierarchy.

sustain tumor growth and are unable to undergo the Imp-to-Syp transition. We conclude that *grh* down-regulation, as a consequence of *trx* inactivation, blocks temporal progression, leading to an expansion of the CSC pool.

As the inactivation of *trr*, *Utx*, and *Set1* did not lead to significant changes in the proportion of Imp^+ tNBs in *pros*^{RNAi} tumors and did not promote tumor growth, we conclude that they do not regulate *grh* or the early temporal patterning genes at the top of the tumor hierarchy. Therefore, the temporal patterning gene network in the tumor context may be a specific target of the Trx/MLL1/2-COMPASS-like complex and not of the other COMPASS complexes.

Although, in our tumor model, *trx* is inactivated from tumor initiation during early larval stages, the additional population of CSCs with embryonic temporal properties is not observed in NB tumors until adult stages (Fig. 9A). This observation also implies that embryonic tNBs originate from the temporal reversion of tNBs with an initial larval temporal identity and not from misregulated temporal transitions in the NB of origin. Temporal reprogramming in Imp^+ tNBs may require several cycles of divisions before the H3K4me³ epigenetic mark becomes diluted, leading to the progressive rewiring of the temporal network (e.g., transcriptional silencing of *grh*). Thus, Imp^+ tNBs in *trx*^{RNAi} tumors exhibit the capacity to revert from larval to embryonic temporal states, revealing plasticity at the apex of the tumor hierarchy (Fig. 9B). A possible explanation for why temporal reversion is not observed in NBs subjected to similar knockdown of epigenetic factors during development is because the window of Imp expression is too short to allow epigenetic reprogramming and rewiring of the temporal gene network. Therefore, permissive conditions for reprogramming may only be met in the tumor context where Imp expression is retained in a subset of tNBs for up to several weeks.

Paralleling the temporal reprogramming in adult stages, we observed that the growth rate of *trx*^{RNAi} tumors appears to accelerate over time. Thus, temporal reprogramming may drive an acceleration of the growth rate, which may also be fueled by the silencing of the *Gadd45* stress pathway. Further work is also needed to decipher the contribution of metabolic reprogramming and other deregulated genes in this process.

Given the conserved function of COMPASS genes during development, it is likely that the mechanisms we describe in the tumorigenic context will also be conserved and relevant for human cancers. In human, inactivating mutations in genes of the MLL1/2-COMPASS-like complex are less frequent than for genes of the MLL3/4-COMPASS-like complex. Moreover, deletion of one MLL1 or MLL2 allele in mice does not induce spontaneous tumorigenesis, unlike haploinsufficiency for MLL3 or MLL4, consistent with inactivation of the MLL1/2-COMPASS-like complex not being responsible for tumor initiation (17). Similarly, in *Drosophila*, *trr* inactivation can initiate tumorigenesis in the gut (52), whereas tumorigenesis upon *trx* inactivation in the gut or any other tissue context has not been reported.

Increasing evidences indicate that human brain tumors follow hierarchical rules driven by deregulated developmental programs (3, 5, 6). Whether and how heterogeneous populations of CSCs coexist in these tumors and are modulated by the genetic background are outstanding questions (69). Our study suggests that inactivation or down-regulation of *trx/MLL1/2* could promote the malignant progression of already established tumors by dysregulating the developmental programs governing their cellular hierarchy. Similarly, it has been proposed that CSC plasticity could underlie

nongenetic adaptive responses to treatment (70). In that respect, inactivation or transcriptional down-regulation of MLL1/2 in hierarchical tumors could induce CSC heterogeneity and facilitate therapeutic resistance by offering the possibility for developmental reversion.

Double-edge effect of PRC2 inactivation

Inactivation of E(z) in *pox*ⁿ>*pros*^{RNAi} tumors also triggers an expansion of the Imp^+ CSC pool in tumors albeit by a different mechanism. There is fewer evidence for reversion toward an embryonic-like temporal identity in *pox*ⁿ>*pros*^{RNAi}, *E(z)*^{RNAi} tumors, as *cas* and *D* remain repressed despite being targets of PRC2-mediated methylation. This is likely to be due to the maintenance of *grh* expression that can repress *cas* in the tumor and is known to be able to repress *D* (71, 72).

Instead, we have observed a strong up-regulation of the lin-28 RNA binding protein in our scRNA-seq experiments. lin-28 mRNA is hardly detected by the scRNA-seq protocol in *control* *pox*ⁿ>*pros*^{RNAi} tumors, although the Lin-28 protein is present in Imp^+ tNBs (20, 32). In contrast, lin-28 mRNA becomes strongly detected under the *pox*ⁿ>*pros*^{RNAi}, *E(z)*^{RNAi} condition by scRNA-seq, a result that was confirmed by immunostaining. Consistently, *lin-28* is a strong target of PcG-mediated repression in late larval NBs as shown by the presence of H3K27me³ repressive mark along its locus. We had previously shown that Lin-28 misexpression triggers higher expression of the Chinmo/Imp oncogenic module in NB tumors (32). We now suspect that this regulatory interaction underlies the expansion of the CSC pool observed in the *E(z)*^{RNAi} tumors.

Unexpectedly, despite an expansion of the CSC pool, *E(z)*^{RNAi} tumors grew much more slowly than *control* NB tumors. We could attribute this phenomenon to the concomitant derepression of proapoptotic or cell cycle exit genes such as *Gadd45* or the *Hox* genes *abd-A* and *Abd-B*. Consistently, preventing apoptosis unleashes the growth potential of tumors with *E(z)* inactivation. This double-edge effect of *E(z)* inactivation (CSC expansion, due to *lin-28* derepression, but reduced growth rate, due to *Hox* and *Gadd45* derepression) calls for a cautious use of EZH2 inhibitors as a therapeutic strategy for treating a number of cancers (18, 73).

It has recently been shown that human LIN28B is also strongly up-regulated upon EZH2 inactivation in human cancers, such as glioblastoma, where it promotes tumor progression (74, 75). Similarly, *Hox* genes and *Imp2* (*Igf2bp2*) are up-regulated in a mouse medulloblastoma model upon Ezh2 inactivation (76). Thus, derepression of the *Imp/lin28* module upon *E(z)/EZH2* inactivation appears to be a highly evolutionarily conserved process that favors tumor growth.

Given that PRC1 and PRC2 proteins cooperate to propagate and maintain the repressive epigenetic marks on histones, it is unexpected that inactivation of PRC1 genes in *pros*^{RNAi} tumors did not lead to similar phenotypes. However, this is consistent with mutations in PRC1 and PRC2 genes affecting different types of cancers in human (11). Alternatively, our knockdown conditions may not be efficient enough to induce a phenotype.

Synergy of *trx* and PRC2 gene inactivation in the tumor context

Whereas coinactivation of *PcG* and *trxG* genes tends to rescue developmental phenotypes during development due to their antagonistic action on canonical target genes, we found that coinactivation of *trx* and *PRC2* genes leads to synergistic effects in the NB tumor

context (exacerbated CSC amplification and tumor growth). This is also in sharp contrast with previous finding showing that EZH2 inhibition counteracts tumors caused by the inactivation of the SWI/SNF or MLL3 complexes, another TrxG complex (60, 61). Thus, our results suggest that inhibition of EZH2 as a therapeutic opportunity for tumors with alterations in *MLL3* or SWI/SNF genes may not be transposable to tumors with inactivated or repressed MLL1/2-COMPASS-like genes. Our experiments have shown that this phenomenon can be explained by two mechanisms. First, coinactivation of *trx* and *PRC2* genes rescues the derepression of *Hox* and *Gadd45* genes induced by PRC2 gene knockdown, as expected for canonical Pcg/trxG targets. Consequently, most apoptosis is abolished in the *PRC2^{RNAi}* *trx^{RNAi}* tumor that can fully deploy its growth potential. Second, in contrast to the apoptotic phenotype, CSC amplification is not abolished by the simultaneous knockdown of *trx* and *PRC2* genes. Instead, CSCs are amplified. Our data suggest that the reversion to an embryonic temporal identity contributes to the phenomenon of CSC amplification and is more efficient in the double-knockdown context than in the single knockdowns. This is likely caused by the combined action of *grh* down-regulation (due to *trx* knockdown) and loss of *cas* and *D* epigenetic repression [due to *E(z)* knockdown]. These two events likely synergize to strongly up-regulate *cas* and *D* expression, stabilizing the embryonic temporal identity. Thus, the subsequent embryonic temporal identity may represent a default temporal state resulting from the cross-regulatory interactions operating among members of the temporal gene network in the absence of epigenetic constraints. Alternatively, derepression of a gene outside of the temporal gene network may interfere with the latter and promote the embryonic-like state.

Our study demonstrates that *trx* and *PRC2* genes are required to promote the unidirectionality of the developmental hierarchy within the tumor context. Their inactivation/knockdown resets a specific developmental program, leading to an altered tumor hierarchy and more aggressive tumors. On the basis of Waddington's representation (77), we propose that coinactivation of *trx* and *PRC2* genes contributes to flattening or erasing the epigenetic landscape guiding temporal transitions and developmental progression at the apex of the tumor hierarchy. Consequently, tumor cells remain locked into a spectrum of CSC states, with reduced opportunities to commit toward the end of their proliferation program (Fig. 9B).

Our work focuses on tumors caused by the inactivation of *pros* in a well-described lineage (*poxⁿ*) that we use as a representative model for NB tumors. We have previously shown that the Imp-to-Syp hierarchy is rather generic among NB tumors as it is also observed when they have different NBs of origin or other initiating genetic alterations (for example, in *brat^{-/-}* and *Snr1^{-/-}* tumors originating from central brain NBs) (20, 32). It remains to be shown that the synergistic effects of COMPASS and PRC2 coinactivation can be generalized to all NB tumors and, more importantly, to human tumors, a reasonable perspective given the known conserved function of these chromatin complexes across species. For example, it will be important to explore how a deregulated balance between *PRC2* and *MLL1/2-COMPASS-like* complexes can reset developmental programs and affect cellular hierarchies and cancer progression. Pediatric brain cancers caused by the down-regulation of EZH2 activity may be sensitive to such a phenomenon (15). Likewise, it will be important to assess how the selection pressure imposed by EZH2 inhibitors could promote the emergence of *MLL1/2* mutant clones and relapse in various cancers.

MATERIALS AND METHODS

Fly strains

Fly stocks were raised at 18°C on standard food (8% cornmeal, 8% yeast, and 1% agar). Unless otherwise stated, crosses were performed at 29°C, and the progeny were maintained at 29°C to maximize RNAi-mediated knockdown efficiency.

The genotype of the tumor driver strain was *UAS-dicer-2; poxⁿ-GAL4, UAS-pros^{RNAi}, UAS-CD8::GFP* or *UAS-dicer2; poxⁿ-GAL4, UAS-pros^{RNAi}, UAS-mCherry^{chinmoUTRs}* (32). *UAS-mCherry^{chinmoUTRs}* was used to assess *chinmo* expression during the screening procedure (coexpressed with *Imp* in the same tNBs) (20, 54). For apoptosis inhibition in tumors, crosses were made at 18°C. Progeny were maintained at 18°C during embryogenesis and switched at 29°C from larval hatching. *UAS-p35* was recombined with *tub-GAL80^{ts}* to prevent inhibition of apoptosis during embryogenesis.

All RNAi lines used had previously been validated in other publications. We validated the efficiency of RNAi lines against PRC1, PRC2, and COMPASS complexes by testing for expected phenotypes in wing discs (fig. S10). Specificity of the observed phenotypes in the tumor context for *E(z)*, *Su(z)12*, *esc*, and *trx* was validated using two different RNAi lines targeting different sequences (Fig. 2, B to D). Strains obtained from the Bloomington Stock Center were as follows: *poxⁿ-GAL4* (BDSC_66685), *UAS-dicer2* (BDSC_24650 and BDSC_24651), *UAS-mCD8::GFP* (BDSC_5130 and BDSC_32185), *tub-GAL80^{ts}* (BDSC_7108), *en-GAL4 UAS-dicer2 UAS-GFP* (BDSC_25752), and *FRT82B trx^{E2}* (BDSC_24160); *FRT2A E(z)⁷³¹* (BDSC_24470), *UAS-E(z)^{RNAi}* (BDSC_27993), *UAS-esc^{RNAi}* (BDSC_31618), *UAS-H3.3K27M* (BDSC_8412), *UAS-pros^{RNAi}* (BDSC_26745), *UAS-Set1^{RNAi}* (BDSC_33704), *UAS-Su(z)12^{RNAi}* (BDSC_31191), *UAS-trx^{RNAi}* (BDSC_29563), *UAS-trx^{RNAi}* (BDSC_31092), *UAS-P35* (BDSC_5072 and BDSC_5073), *UAS-Psc^{RNAi}* (BDSC_31611), and *UAS-sce^{RNAi}* (BDSC_31612); *UAS-grh^{RNAi}* (BDSC_28820) and *UAS-dicer-2, en-GAL4, UAS-GFP* (BDSC_25752). Strains obtained from the Vienna Drosophila RNAi Center (VDRC) were *UAS-E(z)^{RNAi}* (KK107072), *UAS-esc^{RNAi}* (GD5690), *UAS-pros^{RNAi}* (KK101477), *UAS-Su(z)12^{RNAi}* (GD42423), *UAS-trx^{RNAi}* (KK108122), and *UAS-Utx^{RNAi}* (KK105986). The *UAS-abd-A::HA* was provided by Y. Graba and A. Saurin's team. The *UAS-cas* and *UAS-D* stocks were gifts from W. Odenwald (29) and S. Russell, respectively. Mosaic analysis with a repressible cell marker (MARCM) stocks for *FRT2A* and *FRT82B* were as follows: *w¹¹¹⁸, tub-G4 UAS-nGFP-myc hsFLP122; tub-G80LL9, FRT2A/TM6b* and *w¹¹¹⁸; tub-G4 UAS-nGFP-myc hsFLP122; FRT82B tub-G80/TM6c*.

Immunostaining and antibodies

Third instar larval CNSs and adult VNCs were dissected into phosphate-buffered saline (PBS) and fixed with 4% formaldehyde-PBS for 7 min at room temperature. After washes in PBS–0.5% Triton (PBT), samples were incubated for 2 days at 4°C with the following primary antibodies diluted into PBT: anti-Mira (1:50; A. Gould, Francis Crick Institute, London, UK), rabbit anti-Imp (1:500; P. MacDonald), rat anti-Imp and rabbit anti-Syp (1/200 and 1/500, respectively; C. Desplan, New York University, USA), rat or guinea pig anti-Chinmo (both 1:500; N. Sokol, Indiana University, Bloomington, USA), rat anti-Lin-28 (1:500; N. Sokol, Indiana University, Bloomington, USA), rabbit anti-Abd-A (1:250; Y. Graba and A. Saurin, Institut de Biologie du Développement de Marseille, France), rabbit anti-Ubx (1:200; Y. Graba and A. Saurin, Institut de Biologie du Développement de Marseille, France), rabbit anti-PH3

(1:500; Millipore, #06-570), rat anti-PH3 (1:500; Abcam, #ab10543), rat anti-Elav (1:50; Developmental Studies Hybridoma Bank, #9F8A9), chicken anti-GFP (1:1000; Aves, #GFP-1020), rabbit anti-red fluorescent protein (RFP) (1:500; Rockland, #600-401-379), rat anti-RFP (1:500; Chromotek, #5F8), rabbit anti-Dcp1 (1/100; Cell Signaling, #9578), rabbit anti-Cas (1:500; W. Odenwald, National Institutes of Health, USA), guinea pig anti-D (1:50; A. Gould, Francis Crick Institute, London, UK), rabbit anti-D (1/100; S. Russell, University of Cambridge, UK), guinea pig anti-Grh (1/500; W. McGinnis, University of California, San Diego, USA), rabbit anti-H3K27me³ (1:200; Millipore, #07-449), rabbit anti-H3K4me¹ (1/100; Abcam, #ab8895), and rabbit anti-H3K4me³ (1/100; Abcam, #ab8580). After washes in PBT, appropriate combinations of secondary antibodies (Jackson ImmunoResearch, West Grove, PA) were applied overnight at 4°C. DNA was labeled using Hoechst (1 µg/ml). For image acquisition, samples were washed in PBT and then in PBS and mounted into VECTASHIELD (Eurobio, France).

Image acquisition and processing

Images were acquired on the Zeiss LSM 780 confocal microscope with Zen software. Cell counting and tumor volumes were estimated using, respectively, FIJI (Fiji is just Image) Multi-point tool and its 3D Object Counter plugin (78). For figures, the scale is indicated in the figure legends, and all images are single confocal sections unless otherwise stated in the legend.

To compare the mitotic rate of *control* and *trx^{RNAi}* tumors, the average area of tNBs under the two conditions was measured using the segmentation algorithm Cellpose (79) based on the cortical staining of Mira. Segmentation showed that tNBs in *trx^{RNAi}* tumors are, on average, about 20% larger than tNBs under the *control* condition (32.26 µm² versus 27.05 µm², respectively). Extrapolation of the cell area to cell volume, considering tNBs as spheres, leads to an approximate 30% difference (137.25 µm³ versus 105.8 µm³). The total tumor volume for the *trx^{RNAi}* and *control* conditions was divided by the appropriate average cell volume for an approximation of tNB number. For each tumor, the number of PH3⁺ objects was then divided by the calculated number of tNBs and multiplied by 100 to generate the mitotic rate.

Statistical analysis

Quantifications for tumor volume, percentage of Imp⁺ tNBs, the number of PH3⁺ tNBs, and the number of Dcp1⁺ tNBs were repeated identically and independently at least two times and given as dot plots and boxes and whiskers. As in most experiments, less than 30 samples were collected, and each result was statistically analyzed with an appropriate nonparametric statistical test using GraphPad Prism version 8.1.1 for Windows (GraphPad software, La Jolla, CA, USA; www.graphpad.com). A *P* value lower than 0.05 was considered as statistically significant (**P* ≤ 0.05, ***P* ≤ 0.01, ****P* ≤ 0.001, and *****P* ≤ 0.0001).

Preparation of tNBs for scRNA-seq

VNCs from 56 adult females (6 to 8 days old) were dissected for the control condition, VNCs from 45 adult females (5 to 7 days old) were dissected for the *E(z)^{RNAi}* condition, VNCs from 47 adult females (5 to 7 days old) were dissected for the *trx^{RNAi}* condition, and VNCs from 18 adult females (1 to 5 days old) were dissected for the *E(z)^{RNAi}*/*trx^{RNAi}* condition. Following procedures previously described in (20), adult flies were euthanized in 70% ethanol and

washed once in PBS. VNCs were dissected in PBS, collected in a ribonuclease (RNase)-free Protein LoBinding tube filled with ice-cold PBS, and incubated in a freshly prepared dissociation solution containing 0.4% bovine serum albumin (BSA), collagenase I (1 mg/ml), and papain (Sigma-Aldrich) in PBS for 75 min at 29°C with low agitation. Tissues were then disrupted manually by pipetting up and down with a 200-µl tip. Dissociated cells were pelleted for 20 min at 300g at 4°C to remove the dissociation solution and resuspended in ice-cold PBS + 0.4% BSA. The cell suspension was filtered through a 30-µm mesh Pre-Separation Filter (Miltenyi) to remove debris and transferred in a new RNase-free Protein LoBinding tube for FACS sorting. Forty thousand GFP⁺ tNB cells were isolated using a FACSAria II machine (BD) with an 85-µm nozzle, at 310 kPa low pressure, and according to viability, cell size, and GFP intensity. In the next 30 min, sorted cells were encapsulated using the Chromium Single Cell Controller (10x Genomics) for scRNA-seq.

scRNA-seq and analysis

Single cells were processed using the Single cell 3' Library, Gel beads, and multiplex kit (10x Genomics, Pleasanton) as per the manufacturer's protocol. Cells were partitioned into nanoliter-scale Gel Bead-In-Emulsions with the Chromium Single Cell Controller (10x Genomics, Pleasanton), where all generated complementary DNA (cDNA) shares a common 10x barcode. Libraries were generated and sequenced from the cDNA, and the 10x barcodes are used to associate individual reads back to the individual partitions. Analysis using molecular indexing information provides an absolute digital measurement of gene expression levels. Sequencing was performed using a NextSeq 500 Illumina device (one sample) containing a transcript length of 57 base pairs.

Single-cell data processing

Single-cell mRNA sequencing data were analyzed using the 10x Genomics suite Cell Ranger 2.0.1 with default settings for demultiplexing, aligning reads to the *Drosophila* genome (10x Genomics prebuilt dm6 reference genome) with STAR, and counting unique molecular identifiers to build transcriptomic profiles of individual cells. This first level of analysis generates quality metrics (Q30, number of reads by sample...), FASTQ files, and filtered gene matrices. Cell Ranger preprocessing retained 5796 cells with a median number of 1806 genes per cell for the *control* condition (20), 2977 cells with a median number of 1959 genes per cell for the *E(z)^{RNAi}* condition, 2410 cells with a median number of 700 genes per cell for the *trx^{RNAi}* condition, and 3942 cells with a median number of 1190 genes per cell for the *E(z)^{RNAi}*, *trx^{RNAi}* condition. Filtered gene matrices generated via Cell Ranger 2.0.1 were then processed with the R package Seurat v4.0.3, using the online tutorials as guide (<https://satijalab.org/seurat/vignettes.html>) (80). Cell cycle genes were regressed out using the CellCycleScoring and ScaleData functions. Integration of Imp⁺ tNBs of all conditions was performed following the FindIntegrationAnchors function (62). Trajectories and pseudotimes in Figs. 4 and 6 were generated using the SeuratWrappers and Monocle 3 packages (64). Codes for Seurat and Monocle analyses are found in data S4.

SUPPLEMENTARY MATERIALS

Supplementary material for this article is available at <https://science.org/doi/10.1126/sciadv.abi4529>

[View/request a protocol for this paper from Bio-protocol.](#)

REFERENCES AND NOTES

- J. N. Rich, Cancer stem cells: Understanding tumor hierarchy and heterogeneity. *Medicine* **95**, S2–S7 (2016).
- C. E. Meacham, S. J. Morrison, Tumor heterogeneity and cancer cell plasticity. *Nature* **501**, 328–337 (2013).
- J. Gojo, B. Englinger, L. Jiang, J. M. Hübner, M. L. Shaw, O. A. Hack, S. Madlener, D. Kirchhofer, I. Liu, J. Pyrdol, V. Hovestadt, E. Mazzola, N. D. Mathewson, M. Trissal, D. Lötsch, C. Dorfer, C. Haberler, A. Halfmann, L. Mayr, A. Peyrl, R. Geyeregger, B. Schwalm, M. Mauermann, K. W. Pajtler, T. Milde, M. E. Shore, J. E. Geduldig, K. Pelton, T. Czech, O. Ashenberg, K. W. Wucherpfennig, O. Rozenblatt-Rosen, S. Alexandrescu, K. L. Ligon, S. M. Pfister, A. Regev, I. Slavc, W. Berger, M. L. Suva, M. Kool, M. G. Filbin, Single-cell RNA-seq reveals cellular hierarchies and impaired developmental trajectories in pediatric ependymoma. *Cancer Cell* **38**, 44–59.e9 (2020).
- C. Maurange, Temporal patterning in neural progenitors: From *Drosophila* development to childhood cancers. *Dis. Model. Mech.* **13**, dmm044883 (2020).
- I. Tirosi, A. S. Venteicher, C. Hebert, L. E. Escalante, A. P. Patel, K. Yizhak, J. M. Fisher, C. Rodman, C. Mount, M. G. Filbin, C. Neftel, N. Desai, J. Nyman, B. Izar, C. C. Luo, J. M. Francis, A. A. Patel, M. L. Onozato, N. Riggi, K. J. Livak, D. Gennert, R. Satija, B. V. Nahed, W. T. Curry, R. L. Martuza, R. Mylvaganam, A. J. Lafrate, M. P. Frosch, T. R. Golub, M. N. Rivera, G. Getz, O. Rozenblatt-Rosen, D. P. Cahill, M. Monje, B. E. Bernstein, D. N. Louis, A. Regev, M. L. Suva, Single-cell RNA-seq supports a developmental hierarchy in human oligodendrogloma. *Nature* **539**, 309–313 (2016).
- C. P. Couturier, S. Ayyadhyuk, P. U. Le, J. Nadaf, J. Monlong, G. Riva, R. Allache, S. Baig, X. Yan, M. Bourgey, C. Lee, Y. C. D. Wang, V. Wee Yong, M.-C. Guiot, H. Najafabadi, B. Misic, J. Antel, G. Bourque, J. Ragoussis, K. Petrecca, Single-cell RNA-seq reveals that glioblastoma recapitulates a normal neurodevelopmental hierarchy. *Nat. Commun.* **11**, 3406 (2020).
- D. Nassar, C. Blanpain, Cancer stem cells: Basic concepts and therapeutic implications. *Annu. Rev. Pathol.* **11**, 47–76 (2016).
- M. Brand, K. Nakka, J. Zhu, F. J. Dilworth, Polycomb/trithorax antagonism: Cellular memory in stem cell fate and function. *Cell Stem Cell* **24**, 518–533 (2019).
- S. J. Geisler, R. Paro, Trithorax and Polycomb group-dependent regulation: A tale of opposing activities. *Development* **142**, 2876–2887 (2015).
- B. K. Cenik, A. Shilatifard, COMPASS and SWI/SNF complexes in development and disease. *Nat. Rev. Genet.* **22**, 38–58 (2021).
- B. Schüttengruber, H.-M. Bourbon, L. Di Croce, G. Cavalli, Genome regulation by Polycomb and trithorax: 70 years and counting. *Cell* **171**, 34–57 (2017).
- R. D. Hanson, J. L. Hess, B. D. Yu, P. Ernst, M. van Lohuizen, A. Berns, N. M. T. van der Lugt, C. S. Shashikant, F. H. Ruddle, M. Seto, S. J. Korsmeyer, Mammalian trithorax and Polycomb-group homologues are antagonistic regulators of homeotic development. *Proc. Natl. Acad. Sci.* **96**, 14372–14377 (1999).
- P. W. Ingham, Differential expression of bithorax complex genes in the absence of the extra sex combs and trithorax genes. *Nature* **306**, 591–593 (1983).
- J. A. Kassis, J. A. Kennison, J. W. Tamkun, Polycomb and trithorax group genes in *Drosophila*. *Genetics* **206**, 1699–1725 (2017).
- B. Krug, A. S. Harutyunyan, S. Deshmukh, N. Jabado, Polycomb repressive complex 2 in the driver's seat of childhood and young adult brain tumours. *Trends Cell Biol.* **31**, 814–828 (2021).
- C. Kandath, M. D. McLellan, F. Vandin, K. Ye, B. Niu, C. Lu, M. Xie, Q. Zhang, J. F. McMichael, M. A. Wyczalkowski, M. D. M. Leiserson, C. A. Miller, J. S. Welch, M. J. Walter, M. C. Wendt, T. J. Ley, R. K. Wilson, B. J. Raphael, L. Ding, Mutational landscape and significance across 12 major cancer types. *Nature* **502**, 333–339 (2013).
- R. C. Rao, Y. Dou, Hijacked in cancer: The KMT2 (MLL) family of methyltransferases. *Nat. Rev. Cancer* **15**, 334–346 (2015).
- R. Duan, W. Du, W. Guo, EZH2: A novel target for cancer treatment. *J. Hematol. Oncol.* **13**, 104 (2020).
- W. A. Flavahan, E. Gaskell, B. E. Bernstein, Epigenetic plasticity and the hallmarks of cancer. *Science* **357**, eaal2380 (2017).
- S. Genovese, R. Clément, C. Gaultier, F. Besse, K. Narbonne-Reveau, F. Daian, S. Foppolo, N. M. Luis, C. Maurange, Coopted temporal patterning governs cellular hierarchy, heterogeneity and metabolism in *Drosophila* neuroblast tumors. *eLife* **8**, e50375 (2019).
- A. E. Hakes, A. H. Brand, Neural stem cell dynamics: The development of brain tumours. *Curr. Opin. Cell Biol.* **60**, 131–138 (2019).
- C. F. Homem, J. A. Knoblich, *Drosophila* neuroblasts: A model for stem cell biology. *Development* **139**, 4297–4310 (2012).
- C. Q. Doe, Temporal patterning in the *Drosophila* CNS. *Annu. Rev. Cell Dev. Biol.* **33**, 219–240 (2017).
- I. Holguera, C. Desplán, Neuronal specification in space and time. *Science* **362**, 176–180 (2018).
- C. Maurange, L. Cheng, A. P. Gould, Temporal transcription factors and their targets schedule the end of neural proliferation in *Drosophila*. *Cell* **133**, 891–902 (2008).
- T. J. Samuels, A. I. Jarvelin, D. Ish-Horowicz, I. Davis, Imp/IGF2BP levels modulate individual neural stem cell growth and division through myc mRNA stability. *eLife* **9**, e51529 (2020).
- J. W. Truman, M. Bate, Spatial and temporal patterns of neurogenesis in the central nervous system of *Drosophila melanogaster*. *Dev. Biol.* **125**, 145–157 (1988).
- T. Isshiki, B. Pearson, S. Holbrook, C. Q. Doe, *Drosophila* neuroblasts sequentially express transcription factors which specify the temporal identity of their neuronal progeny. *Cell* **106**, 511–521 (2001).
- R. Kambadur, K. Koizumi, C. Stivers, J. Nagle, S. J. Poole, W. F. Odenwald, Regulation of POU genes by *castor* and *hunchback* establishes layered compartments in the *Drosophila* CNS. *Genes Dev.* **12**, 246–260 (1998).
- M. S. Almeida, S. J. Bray, Regulation of post-embryonic neuroblasts by *Drosophila* Grainshead. *Mech. Dev.* **122**, 1282–1293 (2005).
- C. Cenci, A. P. Gould, *Drosophila* Grainshead specifies late programmes of neural proliferation by regulating the mitotic activity and Hox-dependent apoptosis of neuroblasts. *Development* **132**, 3835–3845 (2005).
- K. Narbonne-Reveau, E. Lanet, C. Dillard, S. Foppolo, C. H. Chen, H. Parrinello, S. Riale, N. S. Sokol, C. Maurange, Neural stem cell-encoded temporal patterning delineates an early window of malignant susceptibility in *Drosophila*. *eLife* **5**, 13463 (2016).
- Q. Ren, C.-P. Yang, Z. Liu, K. Sugino, K. Mok, Y. He, M. Ito, A. Nern, H. Otsuna, T. Lee, Stem cell-intrinsic, seven-up-triggered temporal factor gradients diversify intermediate neural progenitors. *Curr. Biol.* **27**, 1303–1313 (2017).
- M. H. Syed, B. Mark, C. Q. Doe, Steroid hormone induction of temporal gene expression in *Drosophila* brain neuroblasts generates neuronal and glial diversity. *eLife* **6**, e26287 (2017).
- Z. Liu, C. P. Yang, K. Sugino, C. C. Fu, L. Y. Liu, X. Yao, L. P. Lee, T. Lee, Opposing intrinsic temporal gradients guide neural stem cell production of varied neuronal fates. *Science* **350**, 317–320 (2015).
- C.-P. Yang, T. J. Samuels, Y. Huang, L. Yang, D. Ish-Horowicz, I. Davis, T. Lee, Imp and Syp RNA-binding proteins govern decommissioning of *Drosophila* neural stem cells. *Development* **144**, 3454–3464 (2017).
- J. Nishino, S. Kim, Y. Zhu, H. Zhu, S. J. Morrison, A network of heterochronic genes including Imp1 regulates temporal changes in stem cell properties. *eLife* **2**, e00924 (2013).
- A. Sagner, I. Zhang, T. Watson, J. Lazaro, M. Melchionda, J. Briscoe, A shared transcriptional code orchestrates temporal patterning of the central nervous system. *PLoS Biol.* **19**, e3001450 (2021).
- L. Tellez, G. Agirman, J. Prados, N. Amberg, S. Fièvre, P. Oberst, G. Bartolini, I. Vitali, C. Cadilhac, S. Hippemeyer, L. Nguyen, A. Dayer, D. Jabaudon, Temporal patterning of apical progenitors and their daughter neurons in the developing neocortex. *Science* **364**, eaav2522 (2019).
- B. Bello, H. Reichert, F. Hirth, The brain tumor gene negatively regulates neural progenitor cell proliferation in the larval central brain of *Drosophila*. *Development* **133**, 2639–2648 (2006).
- J. Betschinger, K. Mechtler, J. A. Knoblich, Asymmetric segregation of the tumor suppressor brat regulates self-renewal in *Drosophila* neural stem cells. *Cell* **124**, 1241–1253 (2006).
- E. Caussinus, C. Gonzalez, Induction of tumor growth by altered stem-cell asymmetric division in *Drosophila melanogaster*. *Nat. Genet.* **37**, 1125–1129 (2005).
- S. P. Choksi, T. D. Southall, T. Bossing, K. Edoff, E. de Wit, B. E. Fischer, B. van Steensel, G. Micklem, A. H. Brand, Prospero acts as a binary switch between self-renewal and differentiation in *Drosophila* neural stem cells. *Dev. Cell* **11**, 775–789 (2006).
- J. Balzeau, M. R. Menezes, S. Cao, J. P. Hagan, The LIN28/let-7 pathway in cancer. *Front. Genet.* **8**, 31 (2017).
- N. Degrauwé, M.-L. Suva, M. Janiszewska, N. Riggi, I. Stamenkovic, IMPs: An RNA-binding protein family that provides a link between stem cell maintenance in normal development and cancer. *Genes Dev.* **30**, 2459–2474 (2016).
- M. D. Abdüsselamoglu, L. Landskron, S. K. Bowman, E. Eroglu, T. Burkard, R. E. Kingston, J. A. Knoblich, Dynamics of activating and repressive histone modifications in *Drosophila* neural stem cell lineages and brain tumors. *Development* **146**, dev183400 (2019).
- B. Bello, N. Holbro, H. Reichert, Polycomb group genes are required for neural stem cell survival in postembryonic neurogenesis of *Drosophila*. *Development* **134**, 1091–1099 (2007).
- H. Komori, Q. Xiao, D. H. Janssens, Y. Dou, C.-Y. Lee, Trithorax maintains the functional heterogeneity of neural stem cells through the transcription factor Buttonhead. *eLife* **3**, e03502 (2014).
- R. A. Neumüller, C. Richter, A. Fischer, M. Novatchkova, K. G. Neumüller, J. A. Knoblich, Genome-wide analysis of self-renewal in *Drosophila* neural stem cells by transgenic RNAi. *Cell Stem Cell* **8**, 580–593 (2011).
- M. Mohan, H.-M. Herz, E. R. Smith, Y. Zhang, J. Jackson, M. P. Washburn, L. Florens, J. C. Eisenberg, A. Shilatifard, The COMPASS family of H3K4 methylases in *Drosophila*. *Mol. Cell. Biol.* **31**, 4310–4318 (2011).

51. A.-K. Classen, B. D. Bunker, K. F. Harvey, T. Vaccari, D. Bilder, A tumor suppressive activity of *Drosophila* Polycomb genes mediated by JAK/STAT signaling. *Nat. Genet.* **41**, 1150–1155 (2009).
52. L. Gervais, M. van den Beek, M. Josserand, J. Sallé, M. Stefanutti, C. N. Perdigoto, P. Skorski, K. Mazouni, O. J. Marshall, A. H. Brand, F. Schweiguth, A. J. Bardin, Stem cell proliferation is kept in check by the chromatin regulators Kismet/CHD7/CHD8 and Trr/MLL3/4. *Dev. Cell* **49**, 556–573.e6 (2019).
53. A.-M. Martinez, B. Schuettengruber, S. Saks, A. Janic, C. Gonzalez, G. Cavalli, Polyhomeotic has a tumor suppressor activity mediated by repression of Notch signaling. *Nat. Genet.* **41**, 1076–1082 (2009).
54. C. Dillard, K. Narbonne-Reveau, S. Foppolo, E. Lanet, C. Maurange, Two distinct mechanisms silence *chinmo* in *Drosophila* neuroblasts and neuroepithelial cells to limit their self-renewal. *Development* **145**, dev154534 (2018).
55. H.-M. Herz, M. Morgan, X. Gao, J. Jackson, R. Rickels, S. K. Swanson, L. Florens, M. P. Washburn, J. C. Eisenberg, A. Shilatifard, Histone H3 lysine-to-methionine mutants as a paradigm to study chromatin signaling. *Science* **345**, 1065–1070 (2014).
56. J. A. Kennison, J. W. Tamkun, Dosage-dependent modifiers of polycomb and antennapedia mutations in *Drosophila*. *Proc. Natl. Acad. Sci.* **85**, 8136–8140 (1988).
57. R. E. Kingston, J. W. Tamkun, Transcriptional regulation by trithorax-group proteins. *Cold Spring Harb. Perspect. Biol.* **6**, a019349 (2014).
58. E. B. Lewis, A gene complex controlling segmentation in *Drosophila*. *Nature* **276**, 565–570 (1978).
59. D. Douillet, C. C. Sze, C. Ryan, A. P. Shah, M. Ugarenko, S. A. Marshall, E. J. Rendleman, D. Zha, K. A. Helmin, Z. Zhao, K. Cao, M. A. Morgan, B. D. Singer, E. Bartom, E. R. Smith, A. Shilatifard, Uncoupling histone H3K4 trimethylation from developmental gene expression via an equilibrium of COMPASS, Polycomb and DNA methylation. *Nat. Genet.* **52**, 615–625 (2020).
60. B. G. Wilson, X. Wang, X. Shen, E. S. McKenna, M. E. Lemieux, Y.-J. Cho, E. C. Koellhoffer, S. L. Pomeroy, S. H. Orkin, C. W. M. Roberts, Epigenetic antagonism between polycomb and SWI/SNF complexes during oncogenic transformation. *Cancer Cell* **18**, 316–328 (2010).
61. L. Wang, Z. Zhao, P. A. Ozark, D. Fantini, S. A. Marshall, E. J. Rendleman, K. A. Cozzolino, N. Louis, X. He, M. A. Morgan, Y. Takahashi, C. K. Collings, E. R. Smith, P. Ntziachristos, J. N. Savas, L. Zou, R. Hashizume, J. J. Meeks, A. Shilatifard, Resetting the epigenetic balance of Polycomb and COMPASS function at enhancers for cancer therapy. *Nat. Med.* **24**, 758–769 (2018).
62. T. Stuart, A. Butler, P. Hoffman, C. Hafemeister, E. Papalexi, W. M. Mauck III, Y. Hao, M. Stoeckius, P. Smibert, R. Satija, Comprehensive integration of single-cell data. *Cell* **177**, 1888–1902.e21 (2019).
63. R. E. Tamura, J. F. de Vasconcellos, D. Sarkar, T. A. Libermann, P. B. Fisher, L. F. Zerbini, GADD45 proteins: Central players in tumorigenesis. *Curr. Mol. Med.* **12**, 634–651 (2012).
64. J. Cao, M. Spielmann, X. Qiu, X. Huang, D. M. Ibrahim, A. J. Hill, F. Zhang, S. Mundlos, L. Christiansen, F. J. Steemers, C. Trapnell, J. Shendure, The single-cell transcriptional landscape of mammalian organogenesis. *Nature* **566**, 496–502 (2019).
65. B. C. Bello, F. Hirth, A. P. Gould, A pulse of the *Drosophila* Hox protein Abdominal-A schedules the end of neural proliferation via neuroblast apoptosis. *Neuron* **37**, 209–219 (2003).
66. F. Bonnay, A. Veloso, V. Steinmann, T. Köcher, M. D. Abdusselamoglu, S. Bajaj, E. Rivelles, L. Landskron, H. Esterbauer, R. P. Zinzen, J. A. Knoblich, Oxidative metabolism drives immortalization of neural stem cells during tumorigenesis. *Cell* **182**, 1490–1507.e19 (2020).
67. J. van den Ameele, A. H. Brand, Neural stem cell temporal patterning and brain tumour growth rely on oxidative phosphorylation. *eLife* **8**, e47887 (2019).
68. S. Zhu, S. Lin, C.-F. Kao, T. Awasaki, A.-S. Chiang, T. Lee, Gradients of the *Drosophila* Chinmo BTB-zinc finger protein govern neuronal temporal identity. *Cell* **127**, 409–422 (2006).
69. R. C. Gimple, S. Bhargava, D. Dixit, J. N. Rich, Glioblastoma stem cells: Lessons from the tumor hierarchy in a lethal cancer. *Genes Dev.* **33**, 591–609 (2019).
70. J.-C. Marine, S.-J. Dawson, M. A. Dawson, Non-genetic mechanisms of therapeutic resistance in cancer. *Nat. Rev. Cancer* **20**, 743–756 (2020).
71. O. A. Bayraktar, C. Q. Doe, Temporal patterning in intermediate progenitors increases neural diversity. *Nature* **498**, 449–455 (2013).
72. M. Nevil, E. R. Bondra, K. N. Schulz, T. Kaplan, M. M. Harrison, Stable binding of the conserved transcription factor grainy head to its target genes throughout *Drosophila melanogaster* development. *Genetics* **205**, 605–620 (2017).
73. K. H. Kim, C. W. M. Roberts, Targeting EZH2 in cancer. *Nat. Med.* **22**, 128–134 (2016).
74. N. A. de Vries, D. Hulsmans, W. Akhtar, J. de Jong, D. C. Miles, M. Blom, O. van Tellingen, J. Jonkers, M. van Lohuizen, Prolonged Ezh2 depletion in glioblastoma causes a robust switch in cell fate resulting in tumor progression. *Cell Rep.* **10**, 383–397 (2015).
75. M. Oshima, N. Hasegawa, M. Mochizuki-Kashio, T. Muto, S. Miyagi, S. Koide, S. Yabata, G. R. Wendt, A. Saraya, C. Wang, K. Shimoda, Y. Suzuki, A. Iwama, Ezh2 regulates the Lin28/let-7 pathway to restrict activation of fetal gene signature in adult hematopoietic stem cells. *Exp. Hematol.* **44**, 282–296.e3 (2016).
76. B. T. Vo, C. Li, M. A. Morgan, I. Theurillat, D. Finkelstein, S. Wright, J. Hyle, S. M. C. Smith, Y. Fan, Y.-D. Wang, G. Wu, B. A. Orr, P. A. Northcott, A. Shilatifard, C. J. Sherr, M. F. Rousset, Inactivation of Ezh2 upregulates Gf1 and drives aggressive Myc-driven group 3 medulloblastoma. *Cell Rep.* **18**, 2907–2917 (2017).
77. C. H. Waddington, *The Strategy of the Genes* (Routledge, 2014).
78. J. Schindelin, I. Arganda-Carreras, E. Frise, V. Kaynig, M. Longair, T. Pietzsch, S. Preibisch, C. Rueden, S. Saalfeld, B. Schmid, J.-Y. Tinnevez, D. J. White, V. Hartenstein, K. Elceir, P. Tomancak, A. Cardona, Fiji: An open-source platform for biological-image analysis. *Nat. Methods* **9**, 676–682 (2012).
79. C. Stringer, T. Wang, M. Michaelos, M. Pachitariu, Cellpose: A generalist algorithm for cellular segmentation. *Nat. Methods* **18**, 100–106 (2021).
80. Y. Hao, S. Hao, E. Andersen-Nissen, W. M. Mauck III, S. Zheng, A. Butler, M. J. Lee, A. J. Wilk, C. Darby, M. Zager, P. Hoffman, M. Stoeckius, E. Papalexi, E. P. Mimitou, J. Jain, A. Srivastava, T. Stuart, L. M. Fleming, B. Yeung, A. J. Rogers, J. M. McElrath, C. A. Bish, R. Gottardo, P. Smibert, R. Satija, Integrated analysis of multimodal single-cell data. *Cell* **184**, 3573–3587.e29 (2021).

Acknowledgments: We thank C. Desplan, A. Gould, W. McGinnis, P. Macdonald, W. Odenwald, S. Russell, A. Saurin, and N. Sokol for flies and antibodies. We are grateful to P. Outters and R. Perbost at HalioDx (Marseille) for generating the single-cell transcriptomic data, P. Grenot at Ciphe for help with FACS, L. Spinelli for help with bioinformatic analysis, and E. Legait for tNB segmentation. We also acknowledge the Bloomington *Drosophila* Stock Center (NIH P40OD018537), the Vienna *Drosophila* RNAi Center (VDRC), TRIP at Harvard Medical School (NIH/NIGMS R01-GM084947), Kyoto DGRC and NIG-Fly Stock Centers for flies, and the Developmental Studies Hybridoma Bank (DSHB) for monoclonal antibodies. We thank France-BioImaging/PICsL infrastructure (ANR-10-INSB-04-01). We thank members of the laboratory for critical reading of the manuscript. **Funding:** This work was supported by Ligue Nationale Contre le Cancer: Labellisation Equipe Ligue (to C.M.), Centre National de la Recherche Scientifique (to C.M. and S.F.), and Ministère de l’Enseignement Supérieur: bourse doctorale (to C.G.). **Author contributions:** Conceptualization: C.G. and C.M. Methodology: C.G. and C.M. Investigation: C.G., S.F., and C.M. Visualization: C.G. and C.M. Supervision: C.M. Writing—original draft: C.G. and C.M. Writing—review and editing: C.G., S.F., and C.M. **Competing interests:** The authors declare that they have no competing interests. **Data and materials availability:** All data needed to evaluate the conclusions in the paper are present in the paper and/or the Supplementary Materials. scRNA-seq data have been deposited in GEO (<https://www.ncbi.nlm.nih.gov/geo>) under accession code GSE179154. All the VDRC *Drosophila* lines can be provided by the Vienna *Drosophila* RNAi Center (VDRC) pending scientific review and a completed material transfer agreement. Requests should be submitted to the VDRC.

Submitted 10 March 2021

Accepted 23 March 2022

Published 11 May 2022

10.1126/sciadv.abi4529